1 **MEMO1 is a Metal Containing Regulator of Iron Homeostasis in Cancer Cells**

2

3 Natalia Dolgova[a*], Eva-Maria E. Uhlemann[a*], Michal T. Boniecki[b*], Frederick S. Vizeacoumar[c*],

4 Martina Ralle[d], Marco Tonelli[e], Syed A. Abbas[a], Jaala Patry[a], Hussain Elhasasna[c], Andrew

5 Freywald[c], Franco J. Vizeacoumar[f,g], and Oleg Y. Dmitriev[a]

6

7

8

9

10

11

12

13

14

15

16

17

18

19

20

21

22

23

[a]Department of Biochemistry, Microbiology and Immunology, University of Saskatchewan, Saskatoon, SK, Canada; [b]Protein Characterization and Crystallization Facility, University of Saskatchewan, Saskatoon, SK, Canada; [c]Department of Pathology and Laboratory Medicine, University of Saskatchewan, Saskatoon, SK, Canada; [d]Department of Molecular and Medical Genetics, Oregon Health and Sciences University, Portland, OR, USA; [e]National Magnetic Resonance Facility at Madison (NMRFAM), University of Wisconsin, Madison, WI, USA; [f]Cancer Research Department, Saskatchewan Cancer Agency, Saskatoon, SK, Canada; [g]Division of Oncology, University of Saskatchewan, Saskatoon, SK, Canada   [*]These authors have contributed equally.

Address correspondence to: oleg.dmitriev@usask.ca or franco.vizeacoumar@usask.ca

Abstract

Mediator of ERBB2-driven Cell Motility 1 (MEMO1) is an evolutionary conserved protein implicated in many biological processes; however, its primary molecular function remains unknown. Importantly, MEMO1 is overexpressed in many types of cancer and was shown to modulate breast cancer metastasis through altered cell motility.

To better understand the function of MEMO1 in cancer cells, we analyzed genetic interactions of MEMO1 using gene essentiality data from 1028 cancer cell lines and found multiple iron-related genes exhibiting genetic relationships with MEMO1. We experimentally confirmed several interactions between MEMO1 and iron-related proteins in living cells or *in vitro*, most notably, the iron transporters transferrin (*TF*), transferrin receptor 2 (*TFR*2), and mitoferrin-2 (*SLC25A28*), and the global iron response regulator IRP1 (*ACO1*). These interactions indicate that cells with high MEMO1 expression levels are hypersensitive to the disruptions in iron distribution. Our data also indicate that MEMO1 is involved in ferroptosis and is linked to iron supply to mitochondria.

We have found that purified MEMO1 binds iron with high affinity under redox conditions mimicking intracellular environment and solved MEMO1 structures in complex with iron and copper. Our work reveals that the iron coordination mode in MEMO1 is very similar to that of iron-containing extradiol dioxygenases, which also display a similar structural fold. We conclude that MEMO1 is an iron-binding protein that regulates iron homeostasis in cancer cells.

Introduction

MEMO1 is a highly conserved protein found in the cytosol of eukaryotic cells from yeast to humans. MEMO1 appears to play a crucial role in cell motility, and has been linked to several biological processes, but its primary function remains unknown. MEMO1 has been implicated in lifespan changes in *C. elegans* and mice (1,2), regulation of vitamin D metabolism (3), and bone and central nervous system development (4-6).

In cancer context, MEMO1 supports the ability of breast tumor cells to invade surrounding tissues, leading to metastasis (7-9). Knockdown of MEMO1 expression reduces breast cancer cell migration in culture, and significantly suppresses lung metastasis in a xenograft model (7). In the clinical setting, retrospective analysis of resected tumors showed a strong correlation between increased expression of MEMO1 and reduced patient survival (7). These effects have been linked to the interaction between the ERBB2 (HER2) receptor and MEMO1, which in turn was proposed to relay the activation of ERBB receptor heterodimers to the microtubule cytoskeleton, thus inducing growth of lamellipodia and enabling cancer cell migration (8). The interaction with ERBB2 gave MEMO1 its name (**M**ediator of **E**RBB2-driven Cell **Mo**tility **1**). MEMO1 also contributes to breast carcinogenesis through the insulin receptor substrate protein 1 (IRS1) pathway (10) and through the interaction with the extranuclear estrogen receptor (11,12).

MEMO1 was shown to catalyze copper-dependent redox reactions, such as superoxide radical production (7). This led to the idea that MEMO1 is required for sustained reactive oxygen species (ROS) production, likely in conjunction with NADPH-oxidase 1 (NOX1) activation. ROS are known to modulate functions of several proteins required for cell motility (13). Alternatively, MEMO1 has been proposed to protect cells from ROS generation by sequestering copper (14). At the same time, sequence homology and structure analyses revealed strong similarity of MEMO1 to iron-containing dioxygenases, redox enzymes that catalyze the incorporation of molecular oxygen into organic molecules (15), suggesting that MEMO1 may have other, iron-dependent, functions in the cell. Strikingly, within the very distinct cluster of four top matches to MEMO1 structure found in the Protein Data Bank using DALI (16), three proved to be iron dioxygenases, with the fourth being a putative dioxygenase.

3

77   Additional clues to MEMO1 function were offered by the genome wide studies of genetic

78   interactions in yeast. *MEMO1* homolog in *S. cerevisiae* is *MHO1*, with 37% amino acid residue

79   identity. In the global network of genetic interactions in yeast (17) , the highest interaction profile

80   similarity was found between *MHO1* and *LSO1*, which encodes a protein strongly induced in

81   response to iron deprivation, and a likely component of the iron transport pathway in yeast (18).

82   Among the five highest scoring hits in the profile similarity search, there was another iron linked

83   protein, the ferredoxin reductase ARH1, an iron-sulfur protein playing an essential role in [2Fe-

84   2S] cluster biogenesis (19). Thus, iron mediated redox reactions emerged as a common MEMO1

85   denominator from two orthogonal bioinformatics approaches, prompting us to investigate its iron

86   connection.

87

88   In the present work, we show that MEMO1 is an iron-binding protein involved in iron

89   metabolism in the cell. Iron has been implicated in carcinogenesis, tumor growth, and metastasis,

90   in particular in breast cancer, by multiple lines of evidence, due to its potentially disruptive role in

91   redox balance in the cell and also because of elevated iron requirements of the rapidly proliferating

92   cancer cells (20,21). Thus, MEMO1 emerges as a direct molecular link between iron metabolism

93   and metastasis in breast cancer.

94

95   **Results**

96   ***MEMO1 displays genetic interactions with multiple iron related proteins***

97   Our analysis of the Cancer Genome Atlas (https://www.cancer.gov/tcga) data reveals that, in

98   addition to breast cancer ($P<10^{-29}$ by Mann-Whitney U-test), MEMO1 is overexpressed in the

99   malignancies of colon, lung and uterine origins ($P<0.0001$), among others, while kidney, head and

100   neck squamous cell tumors and melanoma show little or no difference in median expression levels

101   (Fig. 1A and 1B). Further analyses of MEMO1 levels in breast cancer subtypes determined that

102   MEMO1 overexpression is more prominent in triple negative (TNBC) and HER2+ (HER2

103   enriched) breast tumors than in the luminal subtype (Fig. 1C). This makes MEMO1 a potential

104   therapeutic target in HER2+ breast cancer and, importantly, in TNBC, where few effective

105   treatment options exist, and patient survival is poor. Therefore, we set out to investigate the

106   molecular function of MEMO1.

4

107
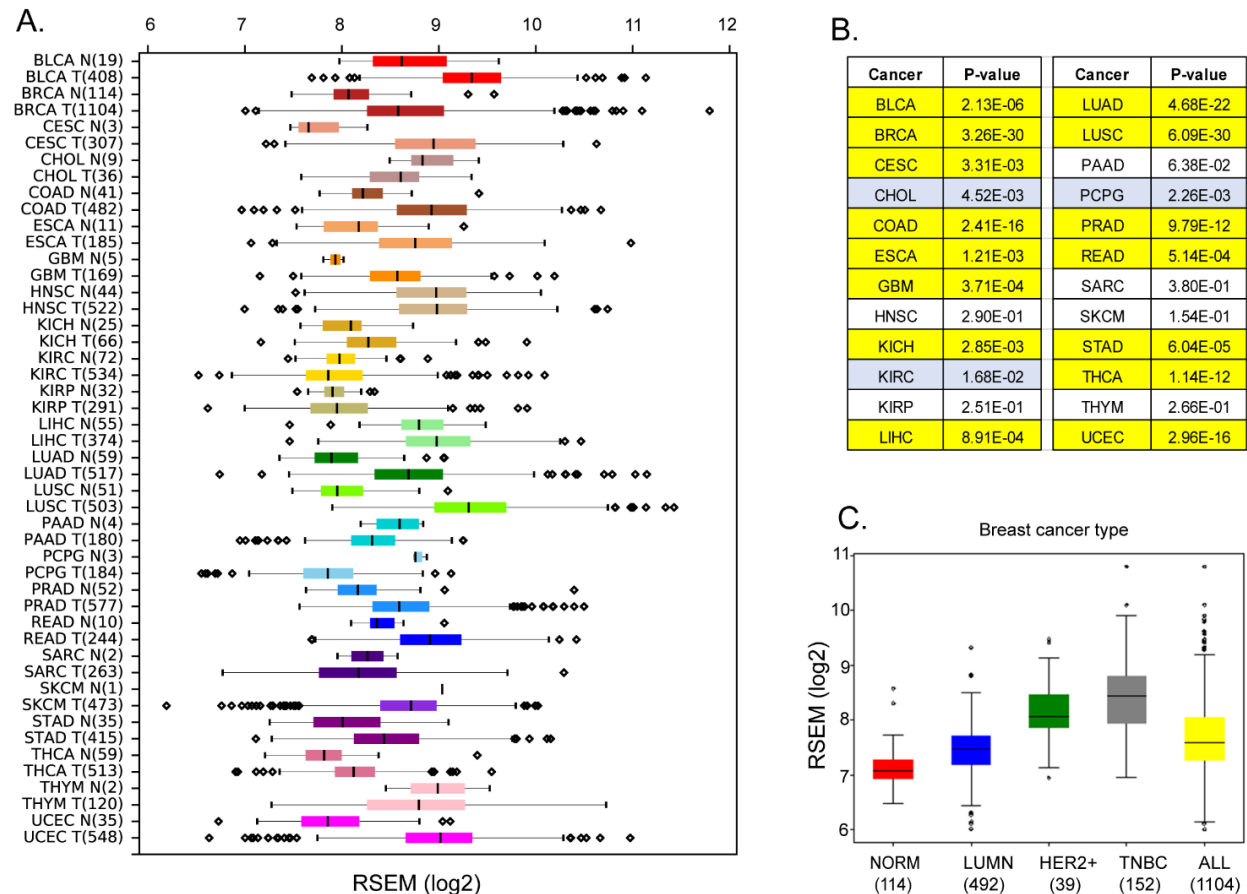
Fig. 1 Expression levels of MEMO1 in tumors and corresponding normal tissue in various malignancies. The data is from the Cancer Genome Atlas (TCGA) database (https://www.cancer.gov/tcga) **(A)** Tissue profile of MEMO1 expression in cancer. Standard TCGA cancer type abbreviations are used (BRCA – breast cancer, SKCM – melanoma). **(B)** Statistically significant differences in MEMO1 expression levels between the tumors and the corresponding normal tissue ($P<0.05$ by Mann-Whitney U-test) are highlighted in *yellow* (higher expression in tumors) or *blue* (lower expression in tumors). **(C)** Subtype analysis of MEMO1 expression in breast cancer, including luminal (*blue*), HER2 positive (*green*) and triple-negative breast cancer (TNBC, *grey*). All differences vs. normal breast tissue (red) are highly significant ($P<10^{-17}$). Note the logarithmic scale (RSEM log$_2$) on the transcript level axis in A and C.

117

Structural similarity of MEMO1 to the iron containing dioxygenases and a clear link between MEMO1 homolog MHO1 and iron metabolism that emerged from genome wide analyses of genetic interactions networks in yeast led us to a hypothesis that MEMO1 plays a role in iron metabolism in cancer cells. As genetic interactions (GIs) are known to be functionally coherent (22), we applied a novel approach to identify GIs of MEMO1 using publicly available gene essentiality data from multiple cell lines. We called a given gene to exhibit GI with MEMO1 if

124 this gene was found to become essential only in cancer cells that either overexpress or
125 downregulate MEMO1. Using previously published genome-wide screens, we analyzed gene
126 essentiality scores derived from 1028 cancer cell lines (23-29) displaying a wide range of MEMO1
127 expression levels.

128

129 This analysis yielded genes that become highly essential (Wilcoxon-rank sum test $P<0.05$),
130 when MEMO1 is either under-expressed, representing GIs identified from loss of function (LOF-
131 GIs), or overexpressed, representing GIs identified from gain of function, (GOF-GIs). Since most
132 of the previous work on MEMO1 and its role in cancer was done in breast cancer cell lines, we
133 analyzed the breast cancer and pan-cancer datasets separately.

134

135 Consistent with the known roles of MEMO1 (30), we found its GIs to be enriched in the
136 following gene sets: Cell Adhesion Molecule Binding (False Discovery Rate, FDR 1.13E-03),
137 Response To Insulin (FDR 2.07E-03), Insulin Signaling Pathway (FDR 6.83E-03), Cellular
138 response to chemical stress (FDR 2.05E-04), ERBB Signaling Pathway (FDR 3.47E-04), and
139 Focal Adhesion (FDR 1.99E-02) (Fig. S1) for LOF-GIs, while gene set enrichment analysis
140 (GSEA) of GOF-GIs identified Signaling by ERBB2 (FDR < 1.00E-05), Microtubule
141 Cytoskeleton Organization (FDR 8.29E-04), Extra-nuclear Estrogen Signaling (FDR 6.13E-04)
142 (Fig. S2). Strong enrichment of the gene sets directly related to the known MEMO1 functions
143 convincingly validated our approach.

144

145 Remarkably, gene set enrichment analysis (GSEA) of the GOF-GIs identified multiple
146 partially overlapping gene sets related to the mitochondrial energy metabolism and redox balance
147 in the cell, including Mitochondrial Transport (FDR, 5.64E-04), Mitochondrial Electron Transport
148 NADH to Ubiquinone (FDR 8.92E-04), Respiratory Electron Transport Chain (FDR 1.54E-02),
149 Citric Acid (TCA) Cycle and Respiratory Electron Transport (FDR 5.99E-03), Oxidative
150 Phosphorylation (FDR 4.32E-02), Glutathione Metabolism (FDR 1.45E-01) and Oxidative Stress
151 Induced Senescence (FDR 1.70E-02) (Fig. S2). These enrichment categories include multiple
152 genes encoding iron containing proteins, as well as those involved in iron-dependent cellular
153 processes, such as ferroptosis. Following this lead, we asked if enrichment of these gene sets in

6

154   the MEMO1 network of the GOF-GIs may reflect specifically high sensitivity of high-MEMO1

155   cancer cells to the disruptions of iron metabolism.

156

157   Further analysis identified sixteen genes encoding proteins involved in iron metabolism and

158   iron transport that showed statistically significant GIs with *MEMO1* (Tables S1 and S2, Fig. S3

159   and S4). Ten genes were found to be more essential in cancer cell lines with high expression of

160   MEMO1 (GOF-GIs, Table S1), while five genes were more essential in the cell lines with low

161   MEMO1 levels (LOF-GIs, Table S2). For example, knockout or knockdown of transferrin receptor

162   2 (TFR2), iron transporter mitoferrin-2 (SLC25A28), or iron response protein (ACO1) selectively

163   suppresses proliferation of the high-MEMO1 cell lines, while knockout of iron transporter DMT1

164   (SLC11A2) leads to a stronger inhibition of proliferation in the cell lines with low MEMO1

165   expression. The other iron related genes showing genetic interactions with *MEMO1* encode

166   mitochondrial proteins that are involved in iron-sulfur cluster biogenesis (*HSPA9, ISCU, FXN,*

167   *ISCA2, NUBPL*), contain iron-sulfur clusters (*ACO2, LIAS*), or are involved in heme synthesis

168   (*HMOX1*). As these results strongly support a link between MEMO1 and iron related proteins, we

169   next explored several of these interactions in more detail.

170

171   ***MEMO1 regulates iron homeostasis in the cell***

172   To confirm the functional link between iron homeostasis and MEMO1 experimentally, we

173   generated clonal MEMO1 knockdowns and knockouts in MDA-MB-231 triple negative breast

174   cancer and A-375 melanoma cell lines using the CRISPR-Cas9 technology and compared the

175   effects of shRNA knockdown of selected genes involved in iron homeostasis on the proliferation

176   rates of the cells with high (parental), low (knockdown) and no (knockout) MEMO1 expression.

177   We chose a melanoma cell line for comparison, because, like breast cancer, it showed a high level

178   of MEMO1 expression, but, unlike breast cancer, there is no statistically significant difference

179   between MEMO1 expression levels in melanoma and normal skin tissue (Fig. 1B). Thus,

180   melanoma serves as a useful benchmark for a cancer, where MEMO1 overexpression is not

181   required to support malignant transformation. In agreement with the previous reports (7,8), we

182   found that MEMO1 knockout in breast cancer cells results in the loss of cell motility as assessed

183   by the wound healing assay (Fig. S5A). MEMO1 knockdown and knockout also decreased overall

184   rates of breast cancer cell proliferation (Fig. S5B). As expected, no strong motility or proliferation

185   rate dependence on MEMO1 expression level was observed in the melanoma cells (Figs. S5C and
186   S5 D).

187
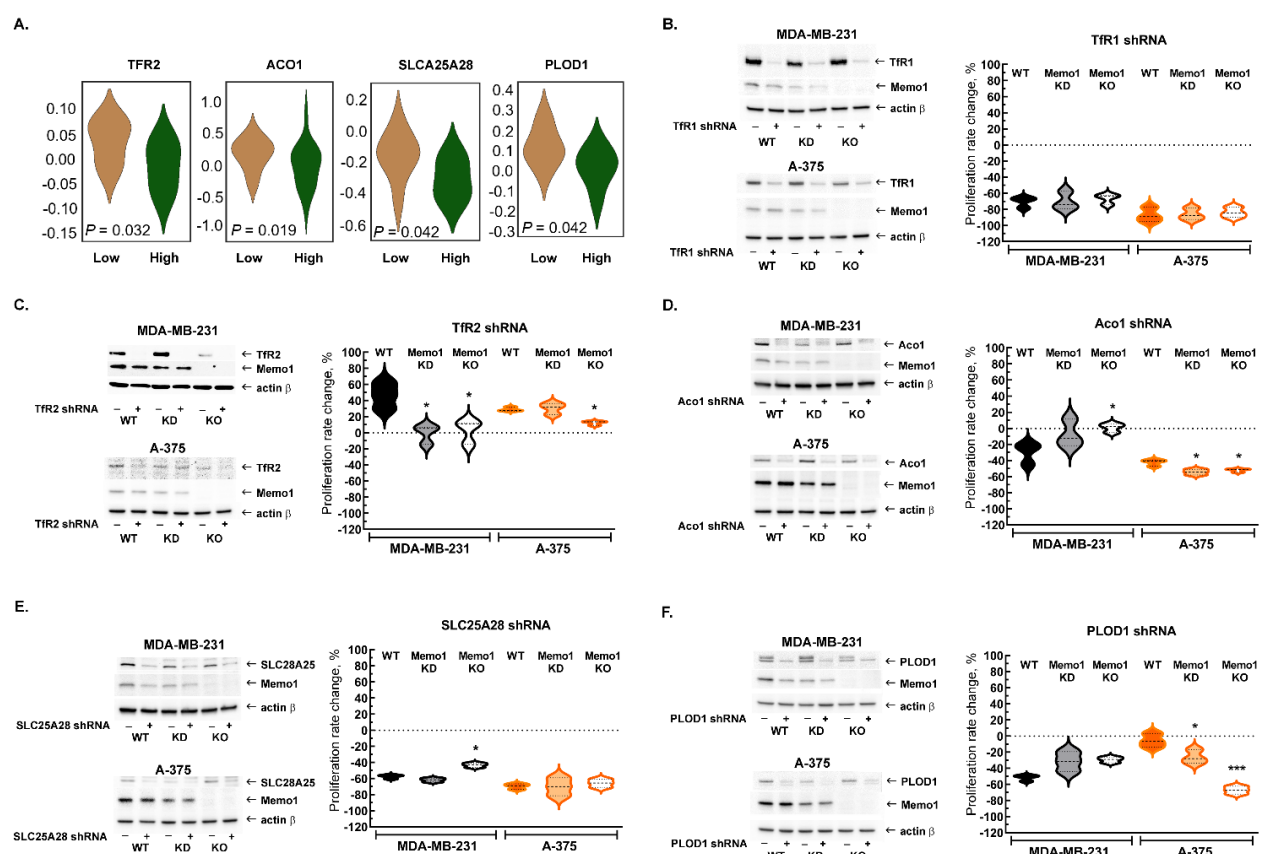
Fig. 2 Interactions between *MEMO1* and iron-related genes. (A) Gene essentiality score distribution for
the selected genes in the high- and low-MEMO1 expressing groups in multiple cancer cell lines as shown
by the database analysis (cf. Table S1). Effects of the TFR1 **(B)**, TFR2 **(C)**, ACO1 **(D)**, SLC25A28 **(E)** and
PLOD1 **(F)** shRNA knockdowns at different MEMO1 expression levels (WT – parental cell line, KD –
MEMO1 knockdown, KO – *MEMO1* knockout). Protein levels were detected by Western blot (*left panels*).
The relative shRNA effect on cell proliferation (*right panels*) is expressed as the difference between the
proliferation rates with the shRNA targeting the gene of interest and the control shRNA (against the red
fluorescent protein) divided by the proliferation rate with the control shRNA.

Because MEMO1 GIs identified by the gene essentiality analysis from 1028 cell lines clearly
suggested a link between MEMO1 and iron transport, we started by investigating the effect of
suppressing transferrin receptors TFR1 and TFR2. TFR1 is the key receptor essential for iron
uptake, while TFR2 appears to be involved in the regulation of iron homeostasis rather than
performing bulk iron uptake (31). TFR2, but not TFR1, was found to exhibit GI with MEMO1
along with other iron-related genes (Fig. 2A). The shRNA targeting *TFR1* decreased TFR1 protein

8

203 expression by more than 90% and caused near complete proliferation inhibition in all the tested

204 cell lines regardless of MEMO1 expression level (Fig. 2B, S6A and S6B). Thus, TFR1 appears to

205 be an essential protein as its loss is nearly lethal on its own, explaining why *TFR1* was not detected

206 in our *in silico* screening of MEMO1 genetic interactions.

207

208   In contrast to *TFR1*, downregulation of TFR2 by shRNA in the high-MEMO1 breast cancer

209 cell line results in the *activation* of cell proliferation, possibly due to the increased availability of

210 iron. By comparison, breast cancer cells with MEMO1 knockout or knockdown show no

211 proliferation rate change in response to TFR2 shRNA knockdown (Fig. 2C and S6C), indicating

212 that TFR2 has a GOF-GI with MEMO1. A similar MEMO1-dependent growth activation pattern

213 was also observed in melanoma cell lines (Fig. 2C and S6D).

214

215   We have also experimentally tested GIs between *MEMO1* and several other iron-related genes

216 detected in our *in silico* analyses (Fig. 2A) and chosen for their key role in the regulation of iron

217 homeostasis in the cell (*ACO1*), iron transport and processing in mitochondria (*SLC25A28* and

218 *HSPA9*), or a direct link between the known MEMO1 function in modulating cancer cell motility

219 and iron (*PLOD1*). *ACO1, SLC25A28* and *PLOD1* showed GOF interactions with MEMO1 in

220 breast cancer cells. Remarkably, *ACO1* knockdown only inhibited proliferation of the high-

221 MEMO1 cells, but not MEMO1 knockout breast cancer cells (Fig. 2D), while *SLC25A28* (Fig. 2E

222 and S7A) and *PLOD1* (Fig. 2F and S8A) knockdowns showed some effect in all cell lines, but a

223 stronger inhibition in the high-MEMO1 cells than in MEMO1 knockout. By comparison, none of

224 the three genes showed GOF interactions in melanoma cells (Fig. 2D, 2E, 2F, S7B and S8B). In

225 fact, *ACO1* and *PLOD1* displayed LOF interactions in melanoma. Like TFR1, shRNA knockdown

226 of HSPA9 results in a major proliferation inhibition of breast cancer and, particularly, of melanoma

227 cells, regardless of MEMO1 expression level (Fig. S9).

228

229   Next, we investigated correlations between the expression levels of MEMO1 and the six iron

230 related proteins whose genetic interactions with MEMO1 had been confirmed. Analysis of the

231 gene expression levels in multiple breast cancer cell lines (Fig. 3A, Fig. S10A) revealed weak but

232 statistically highly significant correlations between the levels of MEMO1 and TFR1 (P=4.6E-18),

233 TFR2 (P=1.8E-14) and PLOD1 (P=1.8E-33). By comparison, none of the correlations in

9

234 melanoma exceeded Spearman's rank correlation coefficient of 0.2 (Fig. 3B, Fig. S10B), a

235 common, if arbitrary, correlation detection threshold.

236

237
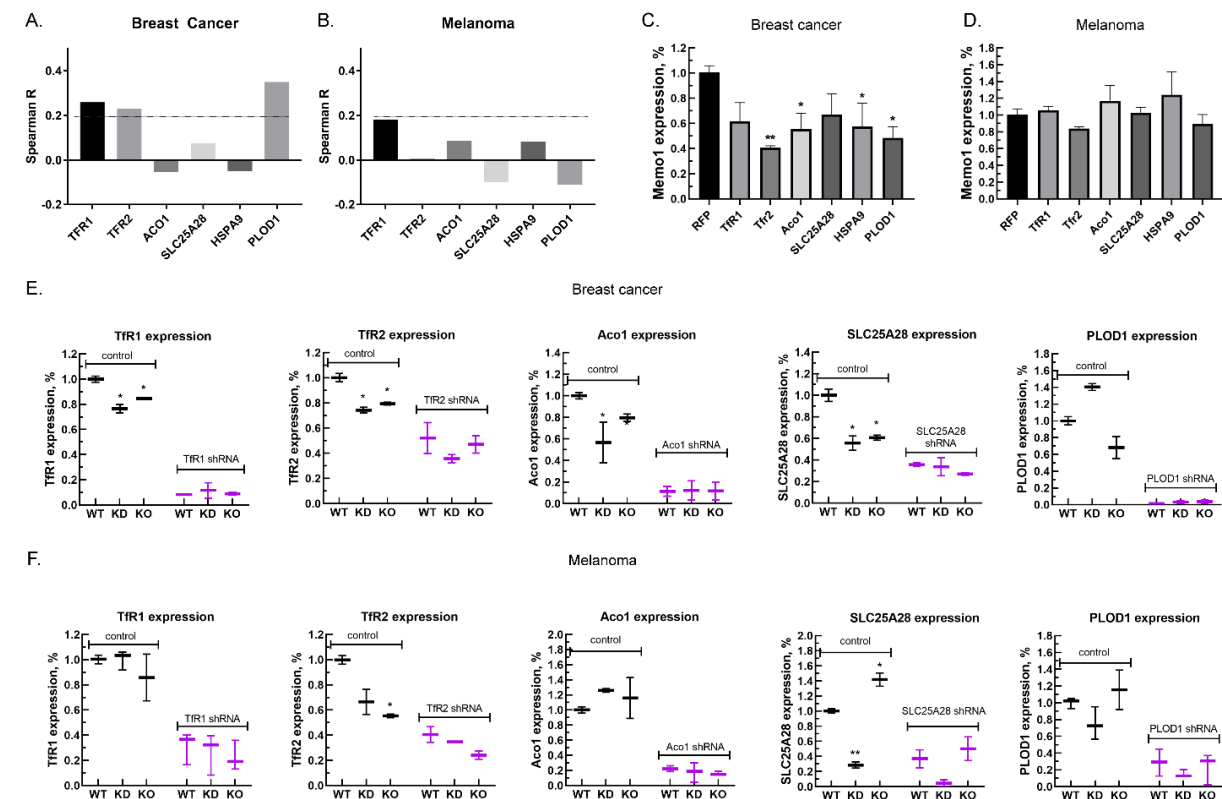
Fig. 3 Relationship between the expression levels of MEMO1 and iron-related proteins in breast cancer and melanoma. (A, B) Correlations between the expression levels of MEMO1 and selected iron related proteins in multiple breast cancer **(A)** and melanoma **(B)** cell lines (cf. Fig. S10) as measured by Spearman rank-order correlation coefficient. **(C, D)** Effect of the selected iron-related shRNA gene knockdowns on MEMO1 levels in breast cancer **(C)** and melanoma **(D)** cell lines detected by Western blot analysis (cf. Fig. 2B - 2F). **(E, F)** Levels of the selected iron-related proteins at various MEMO1 expression levels in breast cancer **(E)** and melanoma **(F)** detected by Western blot analysis in control (shRNA against the red fluorescent protein) and with the shRNA targeting the gene of interest.

246

247 Experimentally, knocking down TFR1, TFR2, ACO1, HSPA9, and PLOD1 in the breast

248 cancer cell line MDA-MB-231 resulted in a decrease in the expression level of MEMO1 by 40-

249 60% (Fig. 3C), but, as expected, no significant effect in the melanoma cell line A-375 was observed

250 (Fig. 3D). Conversely, knockdown or knockout of MEMO1 in breast cancer cells resulted in a

251 statistically significant decrease in the expression levels of TFR1, TFR2, ACO1, and SLC25A28

252 (Fig. 3E). By comparison, MEMO1 knockdown or knockout in melanoma cells decreased only the

10

253   expression level of TFR2 (Fig. 3F), the effect on SLC25A28 knockdown being difficult to

254   interpret. Thus, expression levels of MEMO1 and the other iron-related proteins are correlated in

255   TNBC, suggesting regulation through a common mechanism.

256

257   ***MEMO1 plays an important role in the maintenance of iron concentration in mitochondria***

258   Genetic interactions and expression level correlations between MEMO1 and the iron transport

259   and iron regulating proteins suggested that MEMO1 may also be involved in regulating iron levels

260   in the cell. To test this hypothesis, we measured iron concentration in the cytosol and in the crude

261   mitochondrial fractions of MDA-MB-231 cells in comparison to the same fractions of MEMO1

262   knockdown and knockout cell lines (M67-2 and M67-9). Cells with MEMO1 knockout showed

263   significantly lower iron concentrations in both the cytosolic (Fig. 4A) and the mitochondrial (Fig.

264   4B) fractions. These results suggest that overexpression of MEMO1 allows cells to accumulate

265   higher levels of iron, needed for maintaining the accelerated cell proliferation. This effect may be

266   mediated by a TFR2 - MEMO1 pathway through the iron transport protein transferrin, consistent

267   both with the genetic interactions between MEMO1 and TFR2 and with the physical interaction

268   between the purified MEMO1 and transferrin observed in our experiments by microscale

269   thermophoresis (Fig. 4C). Interestingly, although both *apo*- and *holo*-transferrin bound MEMO1,

270   the *apo*-form showed approximately tenfold higher affinity for MEMO1 (K_d=7.9 × 10^{-9} M)

271   compared to the *holo*-form (K_d=9.7 × 10^{-8} M).

272

273   The decrease in mitochondrial iron in MEMO1-knockout cells taken together with the

274   interactions between MEMO1 and the mitochondrial iron transporter SLC25A28 (mitoferrin-2)

275   prompted us to investigate how MEMO1 knockout affects mitochondria. Mitochondrial

276   morphology in MDA-MB-231 cells with and without MEMO1 knockout was evaluated using

277   mitochondrial marker GRP75 (HSPA9) and the transmembrane electric potential-sensitive dye

278   MitoTracker CM-H2Ros (Fig. 4D). Under basal culture conditions, both the wild type and

279   MEMO1-knockout cell lines display normal mitochondrial shape. By comparison, cells incubated

280   overnight with 1 µM iron chelator deferoxamine (DFX) present normal distribution of

281   mitochondria in the wild type cells, while cells with MEMO1 knockout (M67-9) show perinuclear

282   mitochondrial clustering, as detected both by GRP75 distribution and MitoTracker CM-H_2Ros

283   staining.

11
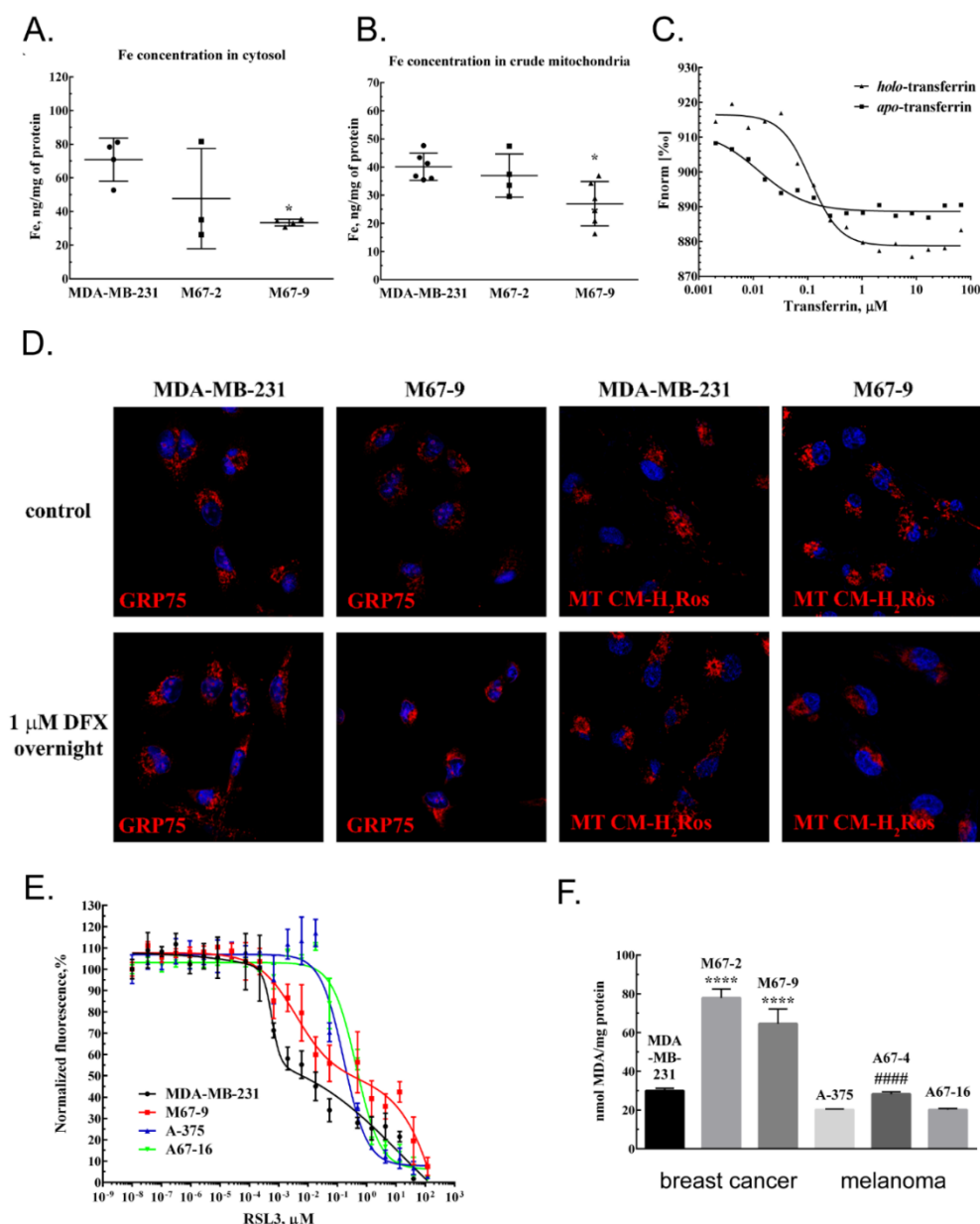
Fig. 4 MEMO1 expression affects iron levels, mitochondrial morphology, and ferroptosis sensitivity of the cells. (A, B) Iron levels in the cytosolic **(A)** and mitochondrial **(B)** fractions from breast cancer cells with high (MDA-MB-231), low (M67-2), and no (M67-9) MEMO1 expression. **(C)** MEMO1 binding to *apo-* and *holo-*transferrin, as measured by the infrared laser-induced thermophoresis. **(D)** MEMO1 knockout in breast cancer cells M67-9 results in perinuclear mitochondrial clustering in the presence of iron chelator deferoxamine (DFX). Mitochondrial marker Grp75 (HSPA9) and MitoTracker CM-H$_2$Ros are *red*, DAPI-stained nuclei are *blue*. **(E)** MEMO1 knockout in breast cancer (M67-9) increases resistance to the ferroptosis inducer RSL3, compared to the parental cell line MDA-MB-231, with an insignificant knockout effect in melanoma (A67-16 and A-375 respectively). **(F)** Malondialdehyde assay shows lower rates of lipid oxidation in the breast cancer cells with high MEMO1 expression (MDA-MB-231) compared to cells with MEMO1 knockout (M67-9) and knockdown (M67-2) cells. The difference is smaller in melanoma cells (A67-4 is MEMO1 knockdown and A67-16 is the knockout).

297 This observation indicates that depletion of labile iron pool caused by the incubation with

298 DFX results in changes in mitochondrial morphology, but only in the cells without MEMO1.

299 Thus, MEMO1 not only plays an important role in overall iron homeostasis in the cell but is

300 specifically involved in iron regulation in mitochondria.

301

302 ***MEMO1 promotes ferroptosis via increase in iron concentration in the cell***

303 As described above, we found that MEMO1 is involved in the regulation of iron concentration

304 in the cells. Elevated iron levels are known to make cells more susceptible to ferroptosis, a type of

305 programmed cell death triggered by the iron-dependent lipid oxidation, and distinct from

306 apoptosis, necrosis, autophagy, and other types of cell death (32). Further suggesting a possible

307 involvement of MEMO1 in ferroptosis, we found GOF-GI between MEMO1 and most of the

308 proteins involved in mitochondria-based ferroptosis (33), including aconitase, VDACs, mitoferrin-

309 2 (SLC25A28), frataxin (FXN), citrate synthase (CS), Acyl-CoA synthetase long-chain family

310 member 4 (ACSL4), sterol carrier protein 2 (SCP2), sirtuin 3 (SIRT3), glutaminase 2 (GLS2),

311 SCO2, and fumarate hydratase (FH) (Supplementary Table S3). To probe the role of MEMO1 in

312 ferroptosis, we compared responses of the wild type and MEMO1-knockout MDA-MB-231 and

313 A-375 cells to the ferroptosis-inducing agent RSL3 (32), a specific inhibitor of glutathione

314 peroxidase 4 (GPX4), the enzyme that resides in mitochondria and plays an essential role in

315 protecting cells against lipid oxidation (34).

316

317 MEMO1 knockout results in a decreased cytotoxicity of RSL3 in breast cancer cells (Fig. 4E),

318 suggesting that high-MEMO1 cells are more sensitive to ferroptosis. Lipid oxidation is one of the

319 hallmarks of ferroptosis. Breast cancer cells with MEMO1 knockdown and knockout have

320 significantly higher levels of lipid oxidation product malondialdehyde (MDA) (Fig. 4F). Taken

321 together, these results indicate that MEMO1 knockout increases ferroptosis resistance in breast

322 cancer cells through the reduced labile iron pool (Fig. 4A and 4B) and a higher tolerance towards

323 lipid oxidation products. Melanoma cells show much smaller MEMO1-dependent variations in the

324 MDA level than breast cancer cells, consistent with the observed smaller difference in RSL3

325 sensitivity between the wild type and MEMO1 knockout in melanoma (Fig. 4E). Overall, these

326 results indicate that MEMO1 overexpression sensitizes breast cancer cells to ferroptosis.

327

13

MEMO1 is an iron-binding protein

We have discovered GIs between MEMO1 and many iron-dependent proteins and found strong indications of MEMO1 involvement in the regulation of iron levels in the cell and in ferroptosis. On the other hand, previous work revealed a putative metal binding site in the structure of MEMO1 (15) and demonstrated that it has copper-dependent redox activity (7). Copper binding to MEMO1 has been demonstrated recently (14). Taken together, these findings prompted us to investigate metal binding properties of MEMO1. We expressed MEMO1 as a fusion with the chitin binding domain and intein and purified the protein by chitin affinity chromatography combined with intein self-cleavage, followed by size exclusion chromatography, producing highly pure, well folded protein, as evidenced by NMR spectroscopy (Fig. S11).

Next, we investigated metal binding to pure MEMO1, in the presence of a mixture of the reduced (GSH) and oxidized (GSSG) glutathione (9.5 mM GSH and 0.5 mM GSSG), approximating redox environment in the cytosol (35). Inductively coupled plasma mass-spectrometry (ICP-MS) showed that, under these conditions, MEMO1 binds stoichiometric amounts of iron (approximately 1:1 molar ratio). In the absence of iron, we have also observed binding of copper (added as Cu(I) to MEMO1 at a molar ratio of copper to protein of approximately 0.4. Under oxidative conditions, without glutathione, or other reducing agents, copper, added as Cu (II), bound to MEMO1 at approximately 0.7 molar ratio.

To determine the metal binding affinity, we measured dissociation constants for iron and copper by isothermal titration calorimetry (ITC). The measured K_d value for iron in the presence of glutathione was $5.0 \pm 2.6 \times 10^{-6}$ M (Fig. 5A) consistent with the value of $2.4 \pm 1.0 \times 10^{-6}$ M determined by microscale thermophoresis (Fig. S12). Glutathione itself binds iron with a K_d of about 10^{-5} M (36), and therefore MEMO1 affinity for free Fe^{2+} ions may be much higher. However, the apparent K_d value measured in the presence of an abundant intracellular low-affinity iron acceptor, such as glutathione, is physiologically more relevant. Copper (I) binding was also detected by ITC, with an estimated K_d of about 3×10^{-6} M (Fig. S13).

14
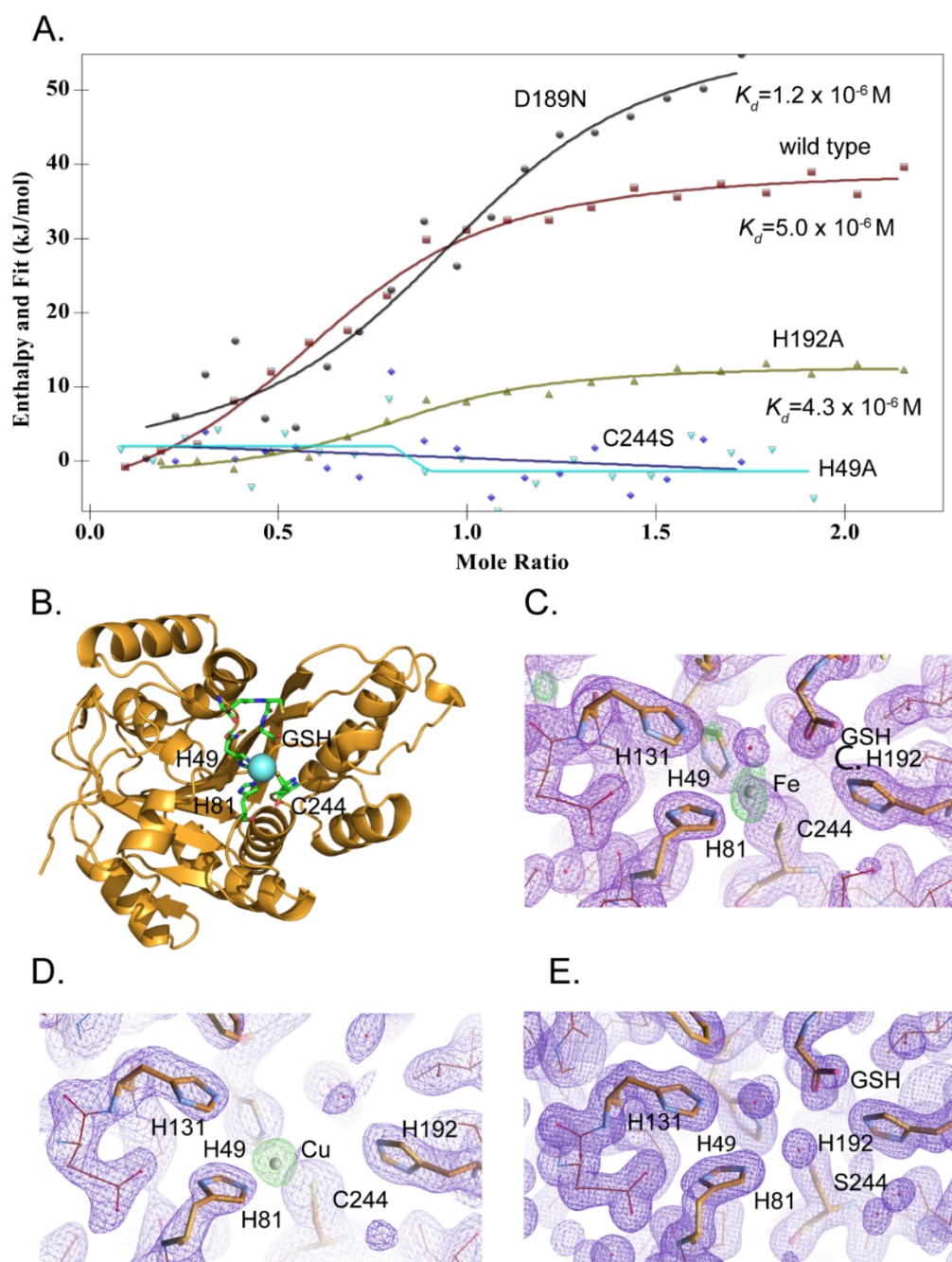
Fig. 5 MEMO1 binds iron or copper in the site formed by H49, H81 and C244. **(A)** Iron binding to the wild type MEMO1 and metal binding site mutants analyzed by isothermal titration calorimetry. Dissociation constant (K_d) values are shown under the fitted binding curves for the wild type (*squares*), D189N (*circles*), and H192A (*triangles*) MEMO1 variants. The C244S (*diamonds*) and H49A (*inverted triangles*) variants did not bind iron. **(B)** Structure of the wild type MEMO1 with iron (PDB ID 7KQ8). **(C, D)** Anomalous difference electron density maps showing iron (7KQ8) **(C)** and copper (7L5C) **(D)** coordinated by H49, H81 and C244. The H131 and H192 residues, albeit close to the metal binding site, do not participate in metal coordination. GSH is glutathione. **(E)** Region of the electron density map of the C244S-MEMO1 (7M8H) corresponding to the metal binding site in the wild type (cf. panels C and D).

15

369   To reveal the binding mode of each metal, we have crystallized MEMO1 in the presence of

370   iron or copper under the conditions similar to those used previously for solving the structure of the

371   metal free protein (15). To prevent metal oxidation, MEMO1 crystallization with iron (II) or

372   copper (I) was set up in an anaerobic chamber and the plates were incubated under argon, while

373   the crystals were growing.   We have solved the structures of MEMO1 with iron (Fig. 5B) at the

374   resolution of 2.15 Å and copper at 2.5 Å, by molecular replacement using the previously solved

375   structure of the metal free protein (PDB ID 3BCZ) (15) (Table S4).   The protein fold of both

376   metal-bound forms of MEMO1 is essentially identical to the metal-free structure, with RMSD for

377   α-carbons of the superimposed structures being less than 0.17 Å. In the MEMO1-Fe structure,

378   iron density is clearly visible in the region of the previously predicted metal-binding site with an

379   overall occupancy of 40-60%, as confirmed by the anomalous diffraction map. Iron is coordinated

380   by H49, H81 and C244 (Fig. 5C). As noted previously, these residues correspond to the iron-

381   coordinating residues H12, H61 and E242 in the structure alignment of MEMO1 with catechol

382   dioxygenase LigB (15), to H12, H59 and E239 in the more recent structure of the bacterial gallate

383   dioxygenase DesB (PDB ID: 3WR8), and to H13, H62 and E251 in the aminophenol dioxygenase

384   from *Comamonas sp*. (PDB ID: 3VSH). Iron coordination by two histidines and an aspartate or

385   glutamate is also observed in many other non-heme dioxygenases (37). Thus, iron coordination by

386   two histidines and a cysteine in MEMO1 is an unusual variation on a common theme. A

387   glutathione molecule was also found in the MEMO1-Fe structure, close to the iron binding site,

388   with the glutathione glycine carboxyl forming an electrostatic interaction with H192. This finding

389   is consistent with Fe-GSH binding to MEMO1 observed by ITC. When MEMO1 was crystallized

390   in the presence of copper, the copper atom bound at the same site, and was coordinated by the

391   same residues as iron (Fig. 5D).

392

393   To confirm the iron binding site, we generated H49A and C244S mutants, along with H192A

394   and D189N variants, because the latter residues are located in the proximity of the bound iron and

395   were previously proposed to belong to the metal binding site of the protein (7). All the mutant

396   proteins were properly folded as shown by NMR (Fig. S11). As shown by ITC (Fig. 5A), iron

397   binding affinity in the H192A and D189N mutants is not significantly changed, whereas H49A

398   and C244S variants do not bind iron at all. Consistent with the crucial role of C244 in metal

399   binding, no metal density was found in the C244S variant of MEMO1 crystallized in the presence

16

400   of copper (Fig 5E). Thus, metal coordination in MEMO1 is achieved by H49, H81 and C244,

401   while H192 and D189 do not participate in metal binding in MEMO1.

402

403   **Discussion**

404   In summary, our results firmly link MEMO1 to a complex network of iron-dependent

405   processes in the cell. We have shown that MEMO1 is an iron binding protein that exhibits GIs

406   with many other iron-related proteins and regulates iron levels in the cell. Since MEMO1 can bind

407   both iron and copper *in vitro*, the question arises, which metal is bound to MEMO1 in the cell. Our

408   K_d measurements suggest that considerations based on the equilibrium dissociation constants

409   should apply to iron binding in the living cell. Concentration of iron in the labile, i.e. readily

410   exchangeable pool, in the cell is within the low micromolar range (38). Therefore, in the absence

411   of competition with another metal, MEMO1 would bind iron from this pool, as we have

412   demonstrated above for glutathione.

413

414   The situation is very different for copper. There is essentially no free or readily exchangeable

415   copper in the cell, as all available copper is tightly bound to proteins with K_d on the order of 10^{-13}

416   M, or less, such as copper chaperones ATOX1 and CCS, metal binding domains of copper

417   ATPases ATP7A and ATP7B, and others (39). Copper transfer between proteins in the cell

418   requires specific protein-protein interactions and is kinetically limited by the rate of such

419   interactions. Therefore, in the absence of specific copper loading mechanisms for MEMO1, it is

420   likely to predominantly bind iron in the cytosol of the living cells, even though copper binding can

421   be observed in *vitro*. Still, consistent with the previous reports (7,14), MEMO1 may bind copper

422   under oxidative conditions in a specific local environment within the cell, and it is tempting to

423   speculate that metal binding change may trigger a switch between different MEMO1 activities in

424   the cell.

425

426   The iron-binding site of MEMO1 is structurally very similar to that of iron-containing

427   extradiol dioxygenases, with a notable difference of a cysteine residue (C244) located at the

428   position occupied by a glutamate in those proteins. No dioxygenase activity has been reported for

429   MEMO1, and we have so far been unable to detect any with a variety of standard substrates we

430   have tried, such as gallate, protocatechuate, 3,4-dihydroxyphenylalanine (L-DOPA), and others.

17

431   Still, the remarkable structural similarity between MEMO1 and dioxygenases strongly suggests

432   that MEMO1 may catalyze redox reactions involved in biosynthesis or breakdown of a signaling

433   molecule in cancer cells.

434

435   We have validated GIs between *MEMO1* and many genes encoding iron-related proteins by

436   studying the effects of loss of function of those gene products on the proliferation of breast cancer

437   and melanoma cell lines with different expression levels of MEMO1. Perhaps the most interesting

438   connection that emerged from these experiments is between MEMO1 and iron transport proteins

439   transferrin and transferrin receptor 2 (TFR2). Both transferrin receptors in human cells, TFR1 and

440   TFR2, are involved in iron transport into the cells. However, whereas TFR1 is an essential protein

441   that accounts for bulk iron uptake, TFR2 plays a regulatory role and appears to protect cells from

442   iron overload (31). Selective activation of high-MEMO breast cancer cell proliferation by TFR2

443   knockdown, taken together with the high-affinity interactions between MEMO1 and transferrin,

444   and a marked decrease in cytosolic iron concentration in the context of MEMO1 knockout suggest

445   an important role for MEMO1 in maintaining iron homeostasis in cancer cells in conjunction with

446   TFR2 (Fig. 6). MEMO1-dependent activation of cell proliferation by TFR2 knockdown, and the

447   link between MEMO1 and TFR2 expression levels is also observed in melanoma cells, suggesting

448   that MEMO1- TFR2 interaction has a salient role in regulating iron in various cell types.

449

450   The link between MEMO1 and iron homeostasis is further supported by the GOF-GI between

451   MEMO1 and the iron-dependent regulatory protein ACO1. ACO1, in its iron-free state, functions

452   as an iron-response protein (IRP1): it binds to the iron-responsive elements (IREs) in the 3'-

453   untranslated regions of mRNA encoding iron transporters TFR1 and DMT1, and in the 5'-

454   untranslated regions of mRNA encoding several other iron dependent proteins, including

455   mitochondrial aconitase ACO2, iron efflux protein FPN1 and iron storage protein ferritin (FTN

456   and FTH subunits) (40). Upon iron binding, IRP1 dissociates from mRNA and becomes a

457   functional cytosolic aconitate hydratase (aconitase). IRP1 dissociation results in the destabilization

458   of TFR1 mRNA and a decrease in iron uptake (41).

459

460

461

18
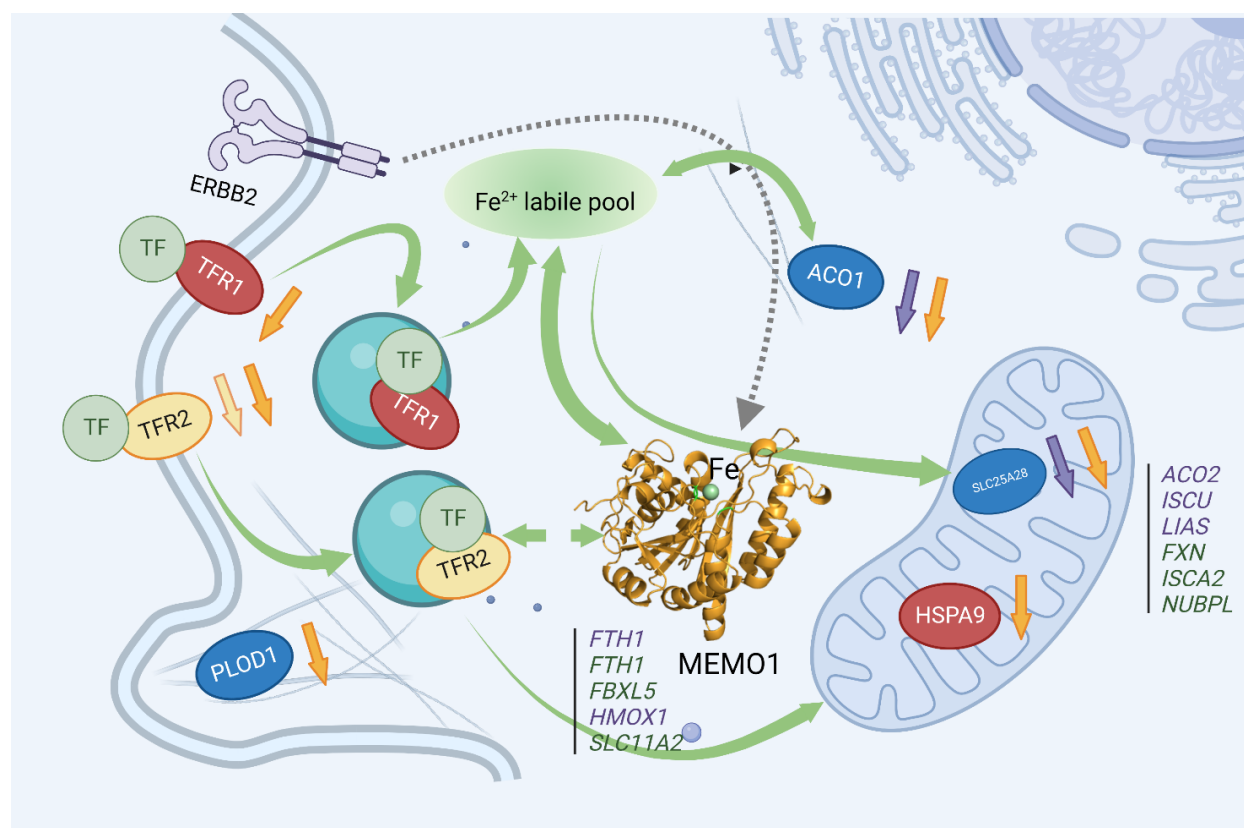
Fig. 6 MEMO1 interactions with the other iron-related proteins in breast cancer cells. Proteins involved in the experimentally validated genetic interactions with MEMO1 in the present work are shown as ovals. Other iron-related genes showing interactions with *MEMO1* by database screening are listed in columns, separately for cytosolic and mitochondrial proteins. Proteins or genes shown in *blue* display SDL interactions with MEMO1; those shown in *green* display SL interactions with MEMO1. In *red* are essential proteins; their knockdown severely inhibits cell proliferation regardless of MEMO1 expression status. TFR2 (*yellow*) knockdown uniquely stimulates proliferation of high-MEMO1 cells. Curved *green* unidirectional arrows show iron transport pathways. Curved *green* bidirectional arrows show iron-dependent regulation. Dashed *grey* arrow indicates MEMO1 interaction with ERBB2 receptor. Short up or down arrows indicate reciprocal effects of the MEMO1 and the interacting genes knockouts and knockdowns: protein expression change in low/no MEMO1 cells is indicated by the same color as the protein, MEMO1 expression change with the protein knockdown is indicated by the *orange* arrow. TF-transferrin.

The selective suppression of the high-MEMO1 cells proliferation by ACO1 knockdown indicates dysregulation of MEMO1-dependent aspects of iron homeostasis in the cell. One of the possible explanations or this finding is a need for a tighter control of iron homeostasis in high-MEMO1 and high-iron cells compared with the cells expressing less MEMO1 and containing less iron. The link between MEMO1 and TFR2, transferrin, and ACO1 would suggest a possible

19

482   interaction between MEMO1 and TFR1. However, TFR1 knockdown strongly inhibited
483   proliferation of all cell lines, regardless of MEMO1 expression levels, consistent with the essential
484   role of TFR1 in iron uptake. Several other genes regulated by ACO1, including DMT1, FTH1, and
485   ACO2 were detected in our database screening, indicating that MEMO1 is an integral part of iron
486   regulatory network of genetic interactions in the cell.

487

488   The MEMO1 iron connection trail leads to mitochondria, as the major intracellular iron
489   consuming organelle. Iron is a cofactor of the highly abundant electron transport proteins in the
490   respiratory chain and several tricarboxylic acid cycle enzymes. It is, therefore, logical to expect
491   that a disruption of iron homeostasis caused by MEMO1 knockout will affect mitochondrial
492   functions. Indeed, we observed that an iron chelator, deferoxamine, causes major changes in the
493   mitochondrial morphology of MEMO1 knockout cells, at a concentration that does not affect the
494   high-MEMO1 parental cells. Perinuclear mitochondrial clustering is one of manifestations of
495   hypoxia (42), which, in turn, may be caused by iron deficiency (40,43). Absence of the perinuclear
496   clustering in the mitochondria of high-MEMO1 cells combined with higher iron level compared
497   to MEMO1 knockouts suggests that MEMO1 specifically facilitates iron transport into
498   mitochondria. MEMO1 overexpression may help to maintain normal metabolism of cancer cells
499   by increasing iron levels in mitochondrial under hypoxic conditions that are frequently found in
500   tumors.

501

502   Remarkably, transferrin and TFR2, which showed physical or genetic interactions with
503   MEMO1 in our work, have been previously reported to be a part of the novel iron transport
504   pathways to mitochondria in substantia nigra dopamine neurons (44) and in erythroid progenitor
505   cells (45). Although it remains to be determined, whether a similar pathway exists in breast cancer
506   cells that we studied, our data provide the first indication that MEMO1, TFR2 and transferrin may
507   all be components of the same iron transport pathway to mitochondria.

508

509   Several proteins involved in the biosynthesis of iron-containing cofactors in mitochondria
510   showed genetic interactions with MEMO1 in our genome-wide *in silico* screening. SLC25A28
511   (Mitoferrin-2), which mediates iron uptake in mitochondria, displayed GOF-GI with MEMO1, its
512   knockdown selectively suppressing proliferation of MEMO1-overexpressing breast cancer cells.

20

513   This may indicate that dysregulation of iron transport processes in high-MEMO1 cells makes them
514   more susceptible to ferroptosis by diverting iron off pathway, to participate in the damaging
515   oxidative reactions.   In fact, in our experiments, high-MEMO1 breast cancer cells were
516   significantly more sensitive to the ferroptosis inducer RSL3 than MEMO1 knockouts.

517

518   Genetic interactions between MEMO1 and PLOD1 in breast cancer cells that we found are
519   particularly notable. PLOD1 is highly expressed in many malignant tumors, likely contributing to
520   the epithelial to mesenchymal cell transition in the course of cancer progression (46). The
521   MEMO1-PLOD1 genetic interaction establishes a direct connection between iron, MEMO1 and
522   cancer cell motility. PLOD1 is an iron-containing enzyme, which participates in the collagen
523   assembly and in the regulation of collagen synthesis and extracellular matrix remodeling,
524   consistent with the established role of MEMO1 in cancer cell tissue invasion and metastasis.

525

526   Many of the GIs between MEMO1 and the other iron-related proteins that we have
527   investigated in the present work manifest themselves not only in MEMO1-dependent effects of
528   the second gene knockdown on cell proliferation, but also in the connections between the
529   expression levels of the two proteins. Such connections are revealed both in the weak but
530   statistically highly significant correlations between the expression levels of MEMO1 and TFR1,
531   TFR2 and PLOD1 across multiple breast cancer cell lines and in the reciprocal effects of gene
532   knockdowns and knockouts on protein expression observed in our experiments. Thus, TFR2 and
533   SLC25A28 (mitoferrin-2) levels are markedly decreased in breast cancer cells with MEMO1
534   knockdown and knockout. Conversely, TFR1, TFR2, SLC25A28 and PLOD1 knockdowns
535   decrease expression levels of MEMO1. These correlations indicate coregulation of expression of
536   many iron-related genes and *MEMO1* (Fig. 6).

537

538   Across the board comparison of MEMO1 genetic interactions and MEMO1 knockout effects
539   between breast cancer and melanoma cells indicates that variations in MEMO1 levels overall have
540   stronger effects in breast cancer cells than in melanoma. Therefore, MEMO1 overexpression
541   relative to the normal tissue rather than absolute MEMO1 levels in the cell appears to be a hallmark
542   of hypersensitivity to iron homeostasis disruption.

543

21

544   In summary, our work has revealed that MEMO1 is an iron-binding protein that regulates

545   iron homeostasis in cancer cells. MEMO1 overexpression may help to maintain normal

546   metabolism of cancer cells by increasing iron levels in mitochondrial under hypoxic conditions.

547   Thus, MEMO1 may serve as a biomarker of tumors particularly sensitive to the therapies targeting

548   iron metabolism in the cell. Genetic interactions of MEMO1 may be targeted to suppress

549   metastasis in breast cancer and other malignancies with high MEMO1 expression level. MEMO1

550   structure and iron coordination mode suggest that it may be involved in the biosynthesis or

551   processing of a signal molecule in the cell.

552

553   **Methods**

554   *Generation of Memo1 knockout and knockdown cell lines* MDA-MB-231 (breast cancer) and

555   A-375 (melanoma) cell lines were obtained from ATCC and cultured in Dulbecco's Modified

556   Eagle Medium (DMEM, HyClone) supplemented with 10% Fetal Bovine Serum (FBS, Gibco).

557   MEMO1 knockdowns and knockouts were generated using CRISPR/Cas9 TrueGuide synthetic

558   crRNA technology (*Invitrogen*) with the guiding crRNA targeting MEMO1 exons 4-6. Genomic

559   cleavage by Cas9 was confirmed using GeneArt Genomic Cleavage Detection kit (*Life*

560   *Technologies*) to amplify the region of genomic DNA targeted for cleavage. Individual clones

561   containing MEMO1 knockouts and knockdowns were generated by limiting dilution and tested for

562   MEMO1 expression by Western blot.

563

564   *Western blotting.* Cells were scraped, washed in PBS, resuspended in lysis buffer (50 mM

565   HEPES, pH 7.4, 150 mM NaCl, 0.2% Triton X-100, cOmplete ULTRA Protease Inhibitor Cocktail

566   (*Roche*) and incubated on ice for 30 min. Nuclei and cell debris were separated by centrifugation

567   at 6,000 g for 10 minutes. Protein concentration in the supernatant was measured by BCA (*Pierce*).

568   Proteins were separated using 4-20% Mini-Protein TGX Precast gels (*Bio-Rad*) and transferred to

569   0.2 μm nitrocellulose membrane (*Bio-Rad*). Membranes were blocked with 5% Amersham ECL

570   Blocking Reagent (*GE*) in PBS with 0.1% Triton X-100 (PBST) for 1 hour at room temperature,

571   then incubated with the primary antibodies at 4°C overnight (see Supplementary Information for

572   the detailed antibody and treatment description). After washing and incubation with the secondary

573   antibody, membranes were washed with 0.5% blocking reagent in PBST (3 times for 5 minutes)

574   and imaged using standard ECL solutions and G:BOX (*Syngene*).

575

576   *Genome wide in-silico screening.* Using a previously described concept (25), we have screened

577   the Marcotte et al (47) and Achilles Project databases (24), and Project DRIVE (27) RNAi datasets

578   and CERES (28,29) CRISPR-Cas9 dataset. The cell lines in each dataset were classified based on

579   the expression of MEMO1 from Cancer Cell Line Encyclopedia (CCLE) (48) database. The

580   difference in the gene essentiality score between the top 5 % of high MEMO1 expressing cell lines

581   and bottom 5 % of low MEMO1 cell lines for pan-cancer and top 25 % of high MEMO1 expressing

582   cell lines and bottom 25 % of low MEMO1 cell lines for breast cancer cell lines were calculated

583   and ranked statistically significant hits (Wilcoxon rank-sum test *P<0.05*) by the difference in

584   median values of the essentiality scores. We thus generated two types of datasets, one containing

585   the genes essential in MEMO1-low cell lines, the other in MEMO1-high cell lines. Collectively,

586   these datasets contained results from 1028 cancer cell lines, including 92 breast cancer cell lines.

587   Enrichment analysis for the SL/SDL interaction partners were performed using Gene Set

588   Enrichment Analysis (GSEA) software (49).

589

590   *The shRNA knockdown assays.* MEMO1 genetic interactions predicted by genome wide gene

591   knockout and knockdown database analysis were validated by measuring proliferation rates of

592   cells with high-level MEMO1 expression (parental cell lines MDA-MB-231 and A-375), MEMO1

593   knockdowns (M67-2 and A67-4 respectively) and complete MEMO1 knockouts (M67-9 and A67-

594   16 respectively) with shRNA knockdowns of PLOD1, HSPA9, SLC25A28, TFR1, TFR2 or

595   ACO1, compared to the control RFP-shRNA. Pooled shRNAs targeting each of the tested genes

596   were delivered into the cells by lentiviral transfection. In brief, cells were transfected with

597   lentivirus and incubated for 24 hours, then the virus was removed, and cells were incubated with

598   puromycin for the next 48 hours, then trypsinyzed and plated onto 96-well plates in the replicates

599   of 8 with at the density of 1,000 cells per well for A-375, A67-4 and A67-16 cells, and 2,000 cells

600   per well for MDA-MB-231, M67-2 and M67-9 in the presence of puromycin. Cells were imaged

601   using Incucyte S3 (*Sartorius*) every 8 hours for the next 120-140 hours. Cell confluency was

602   measured and used to calculate proliferation rates by fitting data using Logistic Growth equation

603   with GraphPad Prizm v. 9. The rest of the cells were plated onto 100 mm plates and harvested for

604   Western blot analysis after 48 hours.

605

23

606   *Cytotoxicity assay.* Cytotoxicity of RSL3 was measured using resazurin assay. Cells were
607 plated onto 96-well plates at the density of 1,000 cell per well for MDA-MB-231 cell line and its
608 derivatives and 750 cell per well for A-375 cell line and its derivatives. The next day cells were
609 titrated with RSL3 and incubated for the next 48 hours. After incubation, media was discarded and
610 replaced by the fresh one containing 88 µM resazurin (*Sigma-Aldrich*). Cells were incubated
611 overnight, and fluorescence was measured using 540 nm excitation and 590 nm emission.

612

613   *Malondialdehyde (MDA) assay.* Cells were grown on 60 mm plates to 80% confluency,
614 harvested and resuspended in 1 ml of cold PBS. A 100 µl volume of suspension was separated for
615 measuring protein concentration by BCA (Pierce). Cells were pelleted at 14,000 g for 1 min, and
616 lipid peroxidation was measured using MDA assay kit (*Abcam*) according to manufacturer's
617 instructions.

618

619   *Immunofluorescence microscopy.* Cells were plated onto glass coverslips at the confluency
620 ~40-50% and incubated overnight. The next day 1 µM of DFX was added and cells were incubated
621 overnight. Following the incubation, cells were washed with cold PBS and fixed using 50:50 mix
622 of methanol and acetone (-20°C) for 30 s, blocked in 5% BSA in PBS overnight and incubated
623 with anti-GRP75 antibodies (D-9, *Santa Cruz Biotechnology*) for 1 h at room temperature. Cells
624 were washed three times with PBS and incubated with secondary goat anti-rabbit antibody labeled
625 with Alexa Fluor 633 (*Invitrogen*) in the dark for 1 h at room temperature. After wash in PBS,
626 cells were mounted onto the glass microscope slides using ProLong Diamond antifade mountant
627 with DAPI (*Invitrogen*) and imaged using Leica Dmi8 confocal microscope after 48 hours.
628   Imaging with MitoTracker CM-H2Ros was performed using live cells: after incubation with
629 DFX the media was removed and substituted with 200 nM MitoTracker solution in DMEM (no
630 FBS), cells were incubated for 30 min, then media was discarded, and cells were incubated for 5
631 min in DMEM without serum. Following that, cells were washed with PBS and incubated in 8 µM
632 Hoechst 33422 (*Invitrogen*) for 10 min, rinsed with PBS, placed in Live Cells Imaging Solution
633 (*Molecular Probes*) and imaged on Leica Dmi8 confocal microscope within 2 hours post staining.

634

635   *ICP-MS measurements.* Cells were grown on 100 mm plates (6 biological replicates), rinsed
636 with PBS, trypsinyzed, then resuspended in 1 ml of cold PBS. A 0.1 ml volume of suspension was

637   kept for determination by BCA (Pierce), the rest was pelleted at 14,000 g for 1 min. Cell pellets

638   were resuspended in 0.4 ml of PBS and lysed by 25 passages through a 27-gauge syringe needle.

639   Cell lysates were centrifuged for 2 minutes at 1,000 g to remove remaining whole cells and nuclei,

640   and the supernatant was centrifuged again at 10,300 g for 10 min. Supernatant containing the

641   cytosolic fraction was collected and centrifuged for 30 min at 100,000 g. Pellet containing crude

642   mitochondrial fraction was resuspended in 0.5 ml of PBS and centrifuged again, then resuspended

643   in 50 μl PBS. Protein concentration in the samples was determined by BCA assay (Pierce). Prior

644   to ICP-MS analysis, the cytosolic fraction was diluted with 1% nitric acid (trace metal grade,

645   Thermo Fisher Scientific). The mitochondrial fraction was briefly digested with concentrated nitric

646   acid (trace metal grade, Thermo Fisher Scientific) at 90°C and subsequently diluted with 1% nitric

647   acid.

648

649   ICP-MS measurements were performed using an Agilent 7700x equipped with an ASX 500

650   autosampler in the OHSU Elemental Analysis Shared Resource (Oregon, USA). Data were

651   quantified using weighed, serial dilutions of a multi-element standard (CEM 2, (VHG Labs VHG-

652   SM70B-100) Fe, Cu, Zn) and a single element standard for Ca (inorganic ventures CGCA1) and

653   P (VHG Labs, PPN-500).

654

655   *Statistical Analysis.* All experiments were repeated at least 3 times; the results are presented as

656   averages ± standard deviation (SD). Statistical significance for the difference between the datasets

657   was calculated using one-way ANOVA with follow-up Tukey's multiple comparison tests or,

658   when appropriate, two-way ANOVA with follow-up Sidak's multiple comparison tests. All

659   calculations were carried out using GraphPad Prizm v. 6. The *P*-values below 0.05 were considered

660   statistically significant. Statistical significance level in the figures is indicated as * or # for *P*<0.05,

661   ** or ## for *P*<0.01, *** or ### for *P*<0.001, and **** or #### for *P*<0.0001.

662

663   *Protein expression and purification.* DNA sequence encoding MEMO1 was codon optimized

664   for *E. coli* expression and prepared by chemical synthesis (*Integrated DNA Technologies, Inc.*).

665   Mutant variants of MEMO1 were generated by site-directed mutagenesis. MEMO1 was expressed

666   as fusion with the chitin-binding domain and intein using vector pTYB12 (*New England BioLabs*)

667   in *E. coli* BL21(DE3) and purified by chitin affinity chromatography combined with intein self-

668 cleavage, essentially as described previously (50). MEMO1 was additionally purified by size

669 exclusion chromatography on a Superdex 75 10/300 GL Increase column (*GE Life Scienc*es) in a

670 buffer containing 50 mM HEPES-Na, pH 7.4, 150 mM NaCl and 0.6 mM *tris*-(2-

671 carboxyethyl)phosphine and concentrated by membrane filtration.

672

673 *Isothermal titration calorimetry.* For ITC experiments, MEMO1 was dialyzed against 50 mM

674 HEPES, pH 7.4, 150 mM NaCl, 9.5 mM reduced glutathione (GSH), 0.5 mM oxidized glutathione

675 (GSSG) under argon. Iron (II) sulfate was dissolved in the used dialysis buffer. ITC was

676 performed on a TA Instruments (New Castle, DE) Low Volume Nano calorimeter using ITCRun

677 software and analyzed with NanoAnalyze software (TA Instruments) using independent model

678 setting. A 0.5 mM solution of iron sulfate was titrated into 0.17 ml of 25 μM MEMO1, 1.5-2.5 μl

679 per injection at 300 s intervals at 25°C under constant stirring at 300 r.p.m. Dilution heat

680 correction was applied by titrating iron sulfate into the ITC buffer containing no protein. Most of

681 the titrations were performed in duplicate or triplicate.

682

683 *Microscale thermophoresis.* Purified MEMO1 was labeled with Red-NHS dye (*NanoTemper*

684 *Technologies GmbH*) and diluted in 10 mM MES, pH 6.0, 250 mM NaCl, 0.1% Pluronic acid.

685 Human holo- and apo-transferrin (*Sigma-Aldrich*) were dissolved the same buffer at a

686 concentration of 0.1-0.15 mM and titrated into 20 nM labeled MEMO1. Measurements were

687 performed on a NanoTemper Monolith NT.115.

688

689 *Protein crystallization.* Protein crystals were obtained by mixing 0.5 μl of purified MEMO1

690 (12-13 mg/mL) with 0.5 μl mother liquor containing 100 mM 2-(N-morpholino) ethanesulfonic

691 acid (MES) pH 5.5-7.0 and 22.5 % PEG-3350 and incubated at 20 °C. Protein crystals that

692 contained reduced Fe^{2+} and Cu^+ were set up inside an anaerobic chamber with 3 ppm of O_2 in the

693 atmosphere of 4 % H_2/N_2 mixture. Mother liquor containing 1 mM metal was incubated inside the

694 chamber with mixing to get rid of oxygen dissolved in solution prior to crystallization. Crystals

695 were harvested and stored in liquid nitrogen using 20 % glycerol as cryoprotectant. Crystals

696 diffracted to 1.75 Å – 2.55 Å and belonged to orthorhombic system, space group $P2_12_12$, with cell

697 dimensions of approximately *a*=140 Å, *b*= 87 Å, *c*=98 Å, α=β=γ=90˚, and contained four

698 molecules in the asymmetric unit.

699

Data collection and structure refinement. Diffraction data were collected at the Canadian Light Source, CMCF section, using beamlines 08ID and 08BM and Pilatus 6M detector. Data were integrated and scaled using XDS package to 2.15 Å (for MEMO1-Fe complex), 2.55 Å (for MEMO1-Cu complex) and 1.75 Å (for MEMO1 C244S mutant) (51). Initial phases were obtained using Phaser MR (52) within ccp4i package and previously solved MEMO1 structure (PDB code: 3BCZ) as a model for molecular replacement (15). The final models of MEMO1 were refined using phenix.refine (53) with manual rebuilding using COOT (54). The coordinates and structure factors have been deposited to the Protein Data Bank with ID codes: 7KQ8 (MEMO1-Fe), 7L5C (MEMO1-Cu), and 7M8H (MEMO1 C244S).

709

Materials availability statement. MEMO1 knockout and knockdown cell lines and MEMO1 expression vectors are available from the authors upon a reasonable request.

712

730

Competing interests

The authors declare that they have no competing interests.

References

1. Ewald, C. Y., Hourihan, J. M., Bland, M. S., Obieglo, C., Katic, I., Moronetti Mazzeo, L. E., Alcedo, J., Blackwell, T. K., and Hynes, N. E. (2017) NADPH oxidase-mediated redox signaling promotes oxidative stress resistance and longevity through memo-1 in C. elegans. *Elife* **6**

2. Haenzi, B., Bonny, O., Masson, R., Lienhard, S., Dey, J. H., M, K.-o., and Hynes, N. E. (2014) Loss of Memo, a novel FGFR regulator, results in reduced lifespan. *FASEB J* **28**, 327-336

3. Moor, M. B., Haenzi, B., Legrand, F., Koesters, R., Hynes, N. E., and Bonny, O. (2018) Renal Memo1 Differentially Regulates the Expression of Vitamin D-Dependent Distal Renal Tubular Calcium Transporters. *Front Physiol* **9**, 874

4. Moor, M. B., Ramakrishnan, S. K., Legrand, F., Dolder, S., Siegrist, M., Durussel, F., Centeno, G., Firsov, D., Hynes, N. E., Hofstetter, W., and Bonny, O. (2018) Redox-Dependent Bone Alkaline Phosphatase Dysfunction Drives Part of the Complex Bone Phenotype in Mice Deficient for Memo1. *JBMR. Plus* **2**, 195-205

5. Nakagawa, N., Plestant, C., Yabuno-Nakagawa, K., Li, J., Lee, J., Huang, C. W., Lee, A., Krupa, O., Adhikari, A., Thompson, S., Rhynes, T., Arevalo, V., Stein, J. L., Molnar, Z., Badache, A., and Anton, E. S. (2019) Memo1-Mediated Tiling of Radial Glial Cells Facilitates Cerebral Cortical Development. *Neuron* **103**, 836-852

6. Van Otterloo, E., Feng, W., Jones, K. L., Hynes, N. E., Clouthier, D. E., Niswander, L., and Williams, T. (2016) MEMO1 drives cranial endochondral ossification and palatogenesis. *Dev. Biol* **415**, 278-295

7. MacDonald, G., Nalvarte, I., Smirnova, T., Vecchi, M., Aceto, N., Dolemeyer, A., Frei, A., Lienhard, S., Wyckoff, J., Hess, D., Seebacher, J., Keusch, J. J., Gut, H., Salaun, D., Mazzarol, G., Disalvatore, D., Bentires-Alj, M., Di Fiore, P. P., Badache, A., and Hynes, N. E. (2014) Memo is a copper-dependent redox protein with an essential role in migration and metastasis. *Sci. Signal* **7**, ra56

8. Marone, R., Hess, D., Dankort, D., Muller, W. J., Hynes, N. E., and Badache, A. (2004) Memo mediates ErbB2-driven cell motility. *Nat. Cell Biol* **6**, 515-522

9. Meira, M., Masson, R., Stagljar, I., Lienhard, S., Maurer, F., Boulay, A., and Hynes, N. E. (2009) Memo is a cofilin-interacting protein that influences PLCgamma1 and cofilin activities, and is essential for maintaining directionality during ErbB2-induced tumor-cell migration. *J. Cell Sci* **122**, 787-797

28

10. Sorokin, A. V., and Chen, J. (2013) MEMO1, a new IRS1-interacting protein, induces epithelial-mesenchymal transition in mammary epithelial cells. *Oncogene* **32**, 3130-3138

11. Frei, A., MacDonald, G., Lund, I., Gustafsson, J. A., Hynes, N. E., and Nalvarte, I. (2016) Memo interacts with c-Src to control Estrogen Receptor alpha sub-cellular localization. *Oncotarget* **7**, 56170-56182

12. Jiang, K., Yang, Z., Cheng, L., Wang, S., Ning, K., Zhou, L., Lin, J., Zhong, H., Wang, L., Li, Y., Huang, J., Zhang, H., and Ye, Q. (2013) Mediator of ERBB2-driven cell motility (MEMO) promotes extranuclear estrogen receptor signaling involving the growth factor receptors IGF1R and ERBB2. *J Biol Chem* **288**, 24590-24599

13. Block, K., and Gorin, Y. (2012) Aiding and abetting roles of NOX oxidases in cellular transformation. *Nat. Rev. Cancer* **12**, 627-637

14. Zhang, X., Walke, G. R., Horvath, I., Kumar, R., Blockhuys, S., Holgersson, S., Walton, P. H., and Wittung-Stafshede, P. (2022) Memo1 binds reduced copper ions, interacts with copper chaperone Atox1, and protects against copper-mediated redox activity in vitro. *Proc Natl Acad Sci U S A* **119**, e2206905119

15. Qiu, C., Lienhard, S., Hynes, N. E., Badache, A., and Leahy, D. J. (2008) Memo is homologous to nonheme iron dioxygenases and binds an ErbB2-derived phosphopeptide in its vestigial active site. *J. Biol. Chem* **283**, 2734-2740

16. Holm, L., and Laakso, L. M. (2016) Dali server update. *Nucleic Acids Res* **44**, W351-W355

17. Costanzo, M., VanderSluis, B., Koch, E. N., Baryshnikova, A., Pons, C., Tan, G., Wang, W., Usaj, M., Hanchard, J., Lee, S. D., Pelechano, V., Styles, E. B., Billmann, M., van, L. J., van, D. N., Lin, Z. Y., Kuzmin, E., Nelson, J., Piotrowski, J. S., Srikumar, T., Bahr, S., Chen, Y., Deshpande, R., Kurat, C. F., Li, S. C., Li, Z., Usaj, M. M., Okada, H., Pascoe, N., San Luis, B. J., Sharifpoor, S., Shuteriqi, E., Simpkins, S. W., Snider, J., Suresh, H. G., Tan, Y., Zhu, H., Malod-Dognin, N., Janjic, V., Przulj, N., Troyanskaya, O. G., Stagljar, I., Xia, T., Ohya, Y., Gingras, A. C., Raught, B., Boutros, M., Steinmetz, L. M., Moore, C. L., Rosebrock, A. P., Caudy, A. A., Myers, C. L., Andrews, B., and Boone, C. (2016) A global genetic interaction network maps a wiring diagram of cellular function. *Science* **353**

18. An, X., Zhang, C., Sclafani, R. A., Seligman, P., and Huang, M. (2015) The late-annotated small ORF LSO1 is a target gene of the iron regulon of Saccharomyces cerevisiae. *Microbiologyopen* **4**, 941-951

19. Braymer, J. J., and Lill, R. (2017) Iron-sulfur cluster biogenesis and trafficking in mitochondria. *J Biol Chem* **292**, 12754-12763

20. Marques, O., da Silva, B. M., Porto, G., and Lopes, C. (2014) Iron homeostasis in breast cancer. *Cancer Lett* **347**, 1-14

21. Torti, S. V., and Torti, F. M. (2013) Iron and cancer: more ore to be mined. *Nat. Rev. Cancer* **13**, 342-355

803 22. Parameswaran, S., Kundapur, D., Vizeacoumar, F. S., Freywald, A., Uppalapati, M., and
804   Vizeacoumar, F. J. (2019) A Road Map to Personalizing Targeted Cancer Therapies Using
805   Synthetic Lethality. *Trends Cancer* **5**, 11-29

806 23. Cheung, H. W., Cowley, G. S., Weir, B. A., Boehm, J. S., Rusin, S., Scott, J. A., East, A.,
807   Ali, L. D., Lizotte, P. H., Wong, T. C., Jiang, G., Hsiao, J., Mermel, C. H., Getz, G.,
808   Barretina, J., Gopal, S., Tamayo, P., Gould, J., Tsherniak, A., Stransky, N., Luo, B., Ren, Y.,
809   Drapkin, R., Bhatia, S. N., Mesirov, J. P., Garraway, L. A., Meyerson, M., Lander, E. S.,
810   Root, D. E., and Hahn, W. C. (2011) Systematic investigation of genetic vulnerabilities
811   across cancer cell lines reveals lineage-specific dependencies in ovarian cancer. *Proc. Natl.*
812   *Acad. Sci. U. S. A* **108**, 12372-12377

813 24. Cowley, G. S., Weir, B. A., Vazquez, F., Tamayo, P., Scott, J. A., Rusin, S., East-Seletsky,
814   A., Ali, L. D., Gerath, W. F., Pantel, S. E., Lizotte, P. H., Jiang, G., Hsiao, J., Tsherniak, A.,
815   Dwinell, E., Aoyama, S., Okamoto, M., Harrington, W., Gelfand, E., Green, T. M., Tomko,
816   M. J., Gopal, S., Wong, T. C., Li, H., Howell, S., Stransky, N., Liefeld, T., Jang, D., Bistline,
817   J., Hill Meyers, B., Armstrong, S. A., Anderson, K. C., Stegmaier, K., Reich, M., Pellman,
818   D., Boehm, J. S., Mesirov, J. P., Golub, T. R., Root, D. E., and Hahn, W. C. (2014) Parallel
819   genome-scale loss of function screens in 216 cancer cell lines for the identification of
820   context-specific genetic dependencies. *Sci Data* **1**, 140035

821 25. Kryukov, G. V., Wilson, F. H., Ruth, J. R., Paulk, J., Tsherniak, A., Marlow, S. E., Vazquez,
822   F., Weir, B. A., Fitzgerald, M. E., Tanaka, M., Bielski, C. M., Scott, J. M., Dennis, C.,
823   Cowley, G. S., Boehm, J. S., Root, D. E., Golub, T. R., Clish, C. B., Bradner, J. E., Hahn, W.
824   C., and Garraway, L. A. (2016) MTAP deletion confers enhanced dependency on the PRMT5
825   arginine methyltransferase in cancer cells. *Science* **351**, 1214-1218

826 26. Marcotte, R., Brown, K. R., Suarez, F., Sayad, A., Karamboulas, K., Krzyzanowski, P. M.,
827   Sircoulomb, F., Medrano, M., Fedyshyn, Y., Koh, J. L. Y., van, D. D., Fedyshyn, B.,
828   Luhova, M., Brito, G. C., Vizeacoumar, F. J., Vizeacoumar, F. S., Datti, A., Kasimer, D.,
829   Buzina, A., Mero, P., Misquitta, C., Normand, J., Haider, M., Ketela, T., Wrana, J. L.,
830   Rottapel, R., Neel, B. G., and Moffat, J. (2012) Essential gene profiles in breast, pancreatic,
831   and ovarian cancer cells. *Cancer Discov* **2**, 172-189

832 27. McDonald, E. R., 3rd, de Weck, A., Schlabach, M. R., Billy, E., Mavrakis, K. J., Hoffman,
833   G. R., Belur, D., Castelletti, D., Frias, E., Gampa, K., Golji, J., Kao, I., Li, L., Megel, P.,
834   Perkins, T. A., Ramadan, N., Ruddy, D. A., Silver, S. J., Sovath, S., Stump, M., Weber, O.,
835   Widmer, R., Yu, J., Yu, K., Yue, Y., Abramowski, D., Ackley, E., Barrett, R., Berger, J.,
836   Bernard, J. L., Billig, R., Brachmann, S. M., Buxton, F., Caothien, R., Caushi, J. X., Chung,
837   F. S., Cortes-Cros, M., deBeaumont, R. S., Delaunay, C., Desplat, A., Duong, W., Dwoske,
838   D. A., Eldridge, R. S., Farsidjani, A., Feng, F., Feng, J., Flemming, D., Forrester, W., Galli,
839   G. G., Gao, Z., Gauter, F., Gibaja, V., Haas, K., Hattenberger, M., Hood, T., Hurov, K. E.,
840   Jagani, Z., Jenal, M., Johnson, J. A., Jones, M. D., Kapoor, A., Korn, J., Liu, J., Liu, Q., Liu,
841   S., Liu, Y., Loo, A. T., Macchi, K. J., Martin, T., McAllister, G., Meyer, A., Molle, S.,
842   Pagliarini, R. A., Phadke, T., Repko, B., Schouwey, T., Shanahan, F., Shen, Q., Stamm, C.,
843   Stephan, C., Stucke, V. M., Tiedt, R., Varadarajan, M., Venkatesan, K., Vitari, A. C.,
844   Wallroth, M., Weiler, J., Zhang, J., Mickanin, C., Myer, V. E., Porter, J. A., Lai, A., Bitter,

H., Lees, E., Keen, N., Kauffmann, A., Stegmeier, F., Hofmann, F., Schmelzle, T., and Sellers, W. R. (2017) Project DRIVE: A Compendium of Cancer Dependencies and Synthetic Lethal Relationships Uncovered by Large-Scale, Deep RNAi Screening. *Cell* **170**, 577-592 e510

28. Meyers, R. M., Bryan, J. G., McFarland, J. M., Weir, B. A., Sizemore, A. E., Xu, H., Dharia, N. V., Montgomery, P. G., Cowley, G. S., Pantel, S., Goodale, A., Lee, Y., Ali, L. D., Jiang, G., Lubonja, R., Harrington, W. F., Strickland, M., Wu, T., Hawes, D. C., Zhivich, V. A., Wyatt, M. R., Kalani, Z., Chang, J. J., Okamoto, M., Stegmaier, K., Golub, T. R., Boehm, J. S., Vazquez, F., Root, D. E., Hahn, W. C., and Tsherniak, A. (2017) Computational correction of copy number effect improves specificity of CRISPR-Cas9 essentiality screens in cancer cells. *Nat. Genet* **49**, 1779-1784

29. Tsherniak, A., Vazquez, F., Montgomery, P. G., Weir, B. A., Kryukov, G., Cowley, G. S., Gill, S., Harrington, W. F., Pantel, S., Krill-Burger, J. M., Meyers, R. M., Ali, L., Goodale, A., Lee, Y., Jiang, G., Hsiao, J., Gerath, W. F. J., Howell, S., Merkel, E., Ghandi, M., Garraway, L. A., Root, D. E., Golub, T. R., Boehm, J. S., and Hahn, W. C. (2017) Defining a Cancer Dependency Map. *Cell* **170**, 564-576

30. Schotanus, M. D., and van Otterloo, E. (2020) Finding MEMO-Emerging Evidence for MEMO1's Function in Development and Disease. *Genes (Basel)* **11**

31. Kawabata, H. (2019) Transferrin and transferrin receptors update. *Free Radic Biol Med* **133**, 46-54

32. Dixon, S. J., Lemberg, K. M., Lamprecht, M. R., Skouta, R., Zaitsev, E. M., Gleason, C. E., Patel, D. N., Bauer, A. J., Cantley, A. M., Yang, W. S., Morrison, B., III, and Stockwell, B. R. (2012) Ferroptosis: an iron-dependent form of nonapoptotic cell death. *Cell* **149**, 1060-1072

33. Wang, H., Liu, C., Zhao, Y., and Gao, G. (2020) Mitochondria regulation in ferroptosis. *Eur J Cell Biol* **99**, 151058

34. Ingold, I., Berndt, C., Schmitt, S., Doll, S., Poschmann, G., Buday, K., Roveri, A., Peng, X., Porto Freitas, F., Seibt, T., Mehr, L., Aichler, M., Walch, A., Lamp, D., Jastroch, M., Miyamoto, S., Wurst, W., Ursini, F., Arner, E. S. J., Fradejas-Villar, N., Schweizer, U., Zischka, H., Friedmann Angeli, J. P., and Conrad, M. (2018) Selenium Utilization by GPX4 Is Required to Prevent Hydroperoxide-Induced Ferroptosis. *Cell* **172**, 409-422 e421

35. Deponte, M. (2013) Glutathione catalysis and the reaction mechanisms of glutathione-dependent enzymes. *Biochim. Biophys. Acta* **1830**, 3217-3266

36. Hider, R. C., and Kong, X. L. (2011) Glutathione: a key component of the cytoplasmic labile iron pool. *Biometals* **24**, 1179-1187

37. Abu-Omar, M. M., Loaiza, A., and Hontzeas, N. (2005) Reaction mechanisms of mononuclear non-heme iron oxygenases. *Chem Rev* **105**, 2227-2252

38. Epsztejn, S., Kakhlon, O., Glickstein, H., Breuer, W., and Cabantchik, I. (1997) Fluorescence analysis of the labile iron pool of mammalian cells. *Anal. Biochem* **248**, 31-40

39. Banci, L., Bertini, I., Ciofi-Baffoni, S., Kozyreva, T., Zovo, K., and Palumaa, P. (2010) Affinity gradients drive copper to cellular destinations. *Nature* **465**, 645-648

40. Lane, D. J., Merlot, A. M., Huang, M. L., Bae, D. H., Jansson, P. J., Sahni, S., Kalinowski, D. S., and Richardson, D. R. (2015) Cellular iron uptake, trafficking and metabolism: Key molecules and mechanisms and their roles in disease. *Biochim Biophys Acta* **1853**, 1130-1144

41. Rouault, T. A., Stout, C. D., Kaptain, S., Harford, J. B., and Klausner, R. D. (1991) Structural relationship between an iron-regulated RNA-binding protein (IRE-BP) and aconitase: functional implications. *Cell* **64**, 881-883

42. Agarwal, S., and Ganesh, S. (2020) Perinuclear mitochondrial clustering, increased ROS levels, and HIF1 are required for the activation of HSF1 by heat stress. *J Cell Sci* **133**

43. Renassia, C., and Peyssonnaux, C. (2019) New insights into the links between hypoxia and iron homeostasis. *Curr Opin Hematol* **26**, 125-130

44. Mastroberardino, P. G., Hoffman, E. K., Horowitz, M. P., Betarbet, R., Taylor, G., Cheng, D., Na, H. M., Gutekunst, C. A., Gearing, M., Trojanowski, J. Q., Anderson, M., Chu, C. T., Peng, J., and Greenamyre, J. T. (2009) A novel transferrin/TfR2-mediated mitochondrial iron transport system is disrupted in Parkinson's disease. *Neurobiol Dis* **34**, 417-431

45. Khalil, S., Holy, M., Grado, S., Fleming, R., Kurita, R., Nakamura, Y., and Goldfarb, A. (2017) A specialized pathway for erythroid iron delivery through lysosomal trafficking of transferrin receptor 2. *Blood Adv* **1**, 1181-1194

46. Wang, Z., Shi, Y., Ying, C., Jiang, Y., and Hu, J. (2021) Hypoxia-induced PLOD1 overexpression contributes to the malignant phenotype of glioblastoma via NF-kappaB signaling. *Oncogene* **40**, 1458-1475

47. Marcotte, R., Sayad, A., Brown, K. R., Sanchez-Garcia, F., Reimand, J., Haider, M., Virtanen, C., Bradner, J. E., Bader, G. D., Mills, G. B., Pe'er, D., Moffat, J., and Neel, B. G. (2016) Functional Genomic Landscape of Human Breast Cancer Drivers, Vulnerabilities, and Resistance. *Cell* **164**, 293-309

48. Barretina, J., Caponigro, G., Stransky, N., Venkatesan, K., Margolin, A. A., Kim, S., Wilson, C. J., Lehar, J., Kryukov, G. V., Sonkin, D., Reddy, A., Liu, M., Murray, L., Berger, M. F., Monahan, J. E., Morais, P., Meltzer, J., Korejwa, A., Jane-Valbuena, J., Mapa, F. A., Thibault, J., Bric-Furlong, E., Raman, P., Shipway, A., Engels, I. H., Cheng, J., Yu, G. K., Yu, J., Aspesi, P., Jr., de Silva, M., Jagtap, K., Jones, M. D., Wang, L., Hatton, C., Palescandolo, E., Gupta, S., Mahan, S., Sougnez, C., Onofrio, R. C., Liefeld, T., MacConaill, L., Winckler, W., Reich, M., Li, N., Mesirov, J. P., Gabriel, S. B., Getz, G., Ardlie, K., Chan, V., Myer, V. E., Weber, B. L., Porter, J., Warmuth, M., Finan, P., Harris, J. L., Meyerson, M., Golub, T. R., Morrissey, M. P., Sellers, W. R., Schlegel, R., and Garraway, L. A. (2012)

32

920   The Cancer Cell Line Encyclopedia enables predictive modelling of anticancer drug
921   sensitivity. *Nature* **483**, 603-607

922 49. Subramanian, A., Tamayo, P., Mootha, V. K., Mukherjee, S., Ebert, B. L., Gillette, M. A.,
923   Paulovich, A., Pomeroy, S. L., Golub, T. R., Lander, E. S., and Mesirov, J. P. (2005) Gene
924   set enrichment analysis: a knowledge-based approach for interpreting genome-wide
925   expression profiles. *Proc Natl Acad Sci U S A* **102**, 15545-15550

926 50. Dmitriev, O., Tsivkovskii, R., Abildgaard, F., Morgan, C. T., Markley, J. L., and Lutsenko,
927   S. (2006) Solution structure of the N-domain of Wilson disease protein: Distinct nucleotide-
928   binding environment and effects of disease mutations. *Proc. Natl. Acad. Sci. U. S. A* **103**,
929   5302-5307

930 51. Kabsch, W. (2010) Xds. *Acta Crystallogr D Biol Crystallogr* **66**, 125-132

931 52. McCoy, A. J., Grosse-Kunstleve, R. W., Adams, P. D., Winn, M. D., Storoni, L. C., and
932   Read, R. J. (2007) Phaser crystallographic software. *J Appl Crystallogr* **40**, 658-674

933 53. Liebschner, D., Afonine, P. V., Baker, M. L., Bunkoczi, G., Chen, V. B., Croll, T. I., Hintze,
934   B., Hung, L. W., Jain, S., McCoy, A. J., Moriarty, N. W., Oeffner, R. D., Poon, B. K.,
935   Prisant, M. G., Read, R. J., Richardson, J. S., Richardson, D. C., Sammito, M. D., Sobolev,
936   O. V., Stockwell, D. H., Terwilliger, T. C., Urzhumtsev, A. G., Videau, L. L., Williams, C.
937   J., and Adams, P. D. (2019) Macromolecular structure determination using X-rays, neutrons
938   and electrons: recent developments in Phenix. *Acta Crystallogr D Struct Biol* **75**, 861-877

939 54. Emsley, P., Lohkamp, B., Scott, W. G., and Cowtan, K. (2010) Features and development of
940   Coot. *Acta Crystallogr D Biol Crystallogr* **66**, 486-501

941

Supplementary information
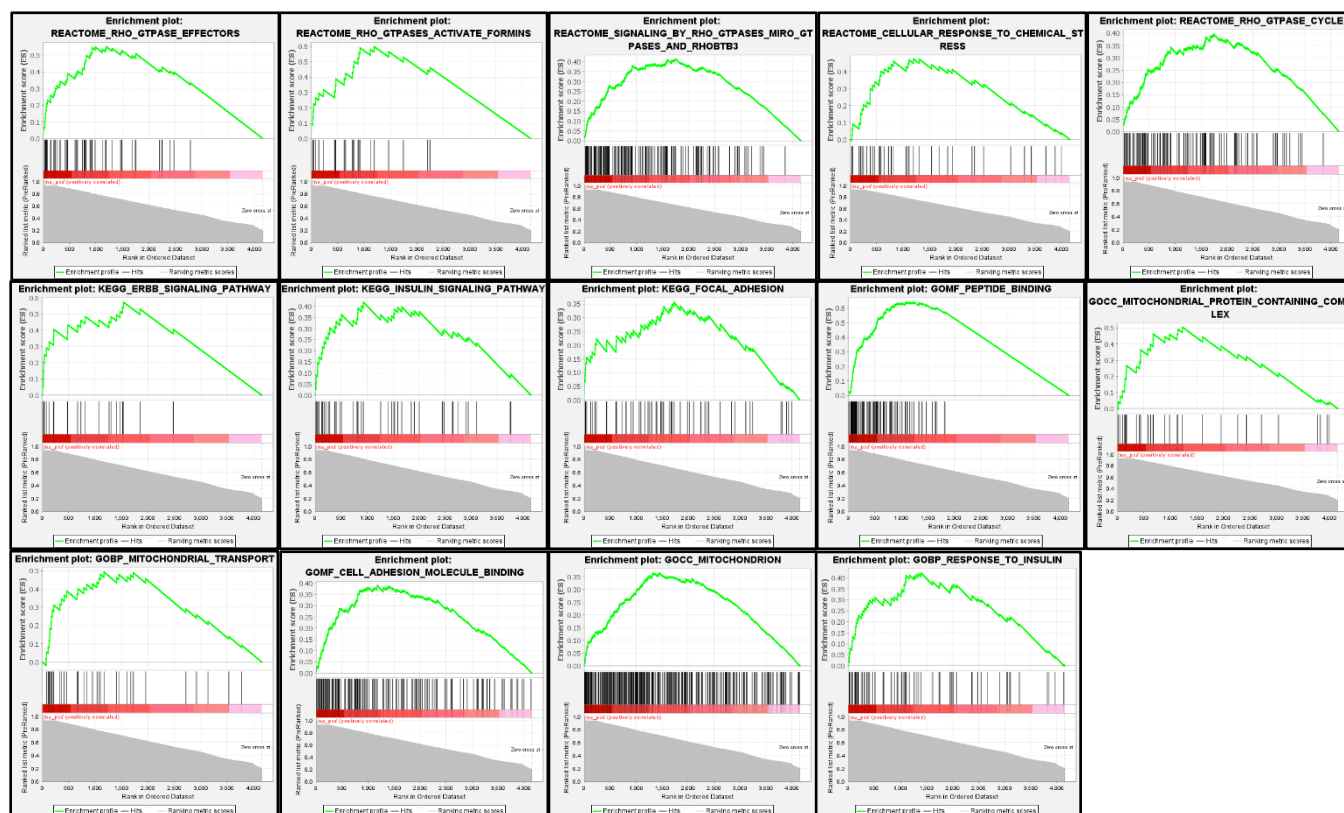
Fig. S1 Enrichment plots for MEMO1 loss of function genetic interaction hits
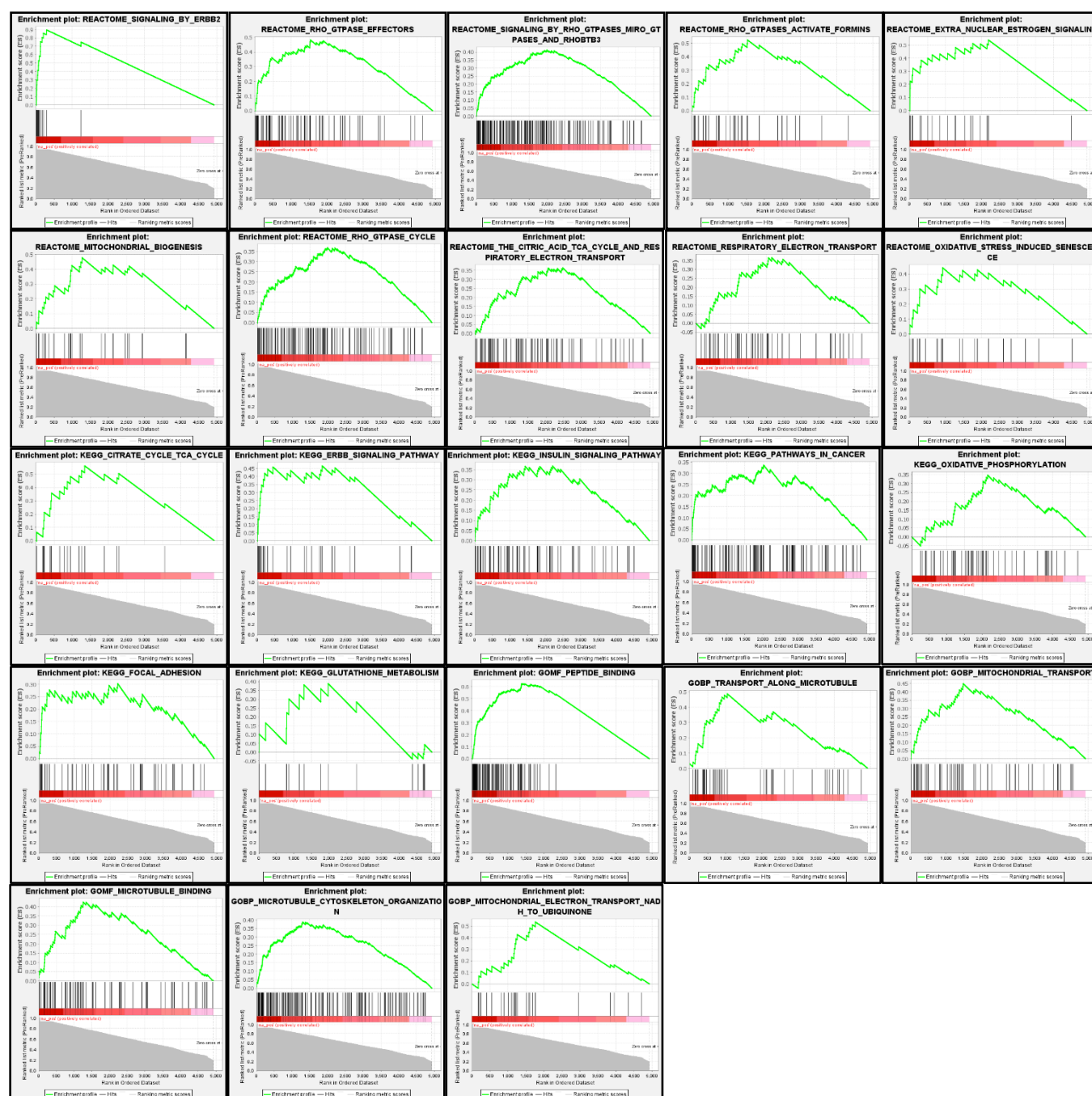
Fig. S2 Enrichment plots for MEMO1 gain of function genetic interactions hits

Cell lines with low MEMO1 expression

Cell lines with high MEMO1 expression

Fig. S3 Iron related genes exhibiting GOF interactions with MEMO1. Gene essentiality score distribution in the low- and high-MEMO1 expressing groups with the number of cell lines in each group is shown (cf. Table S1).
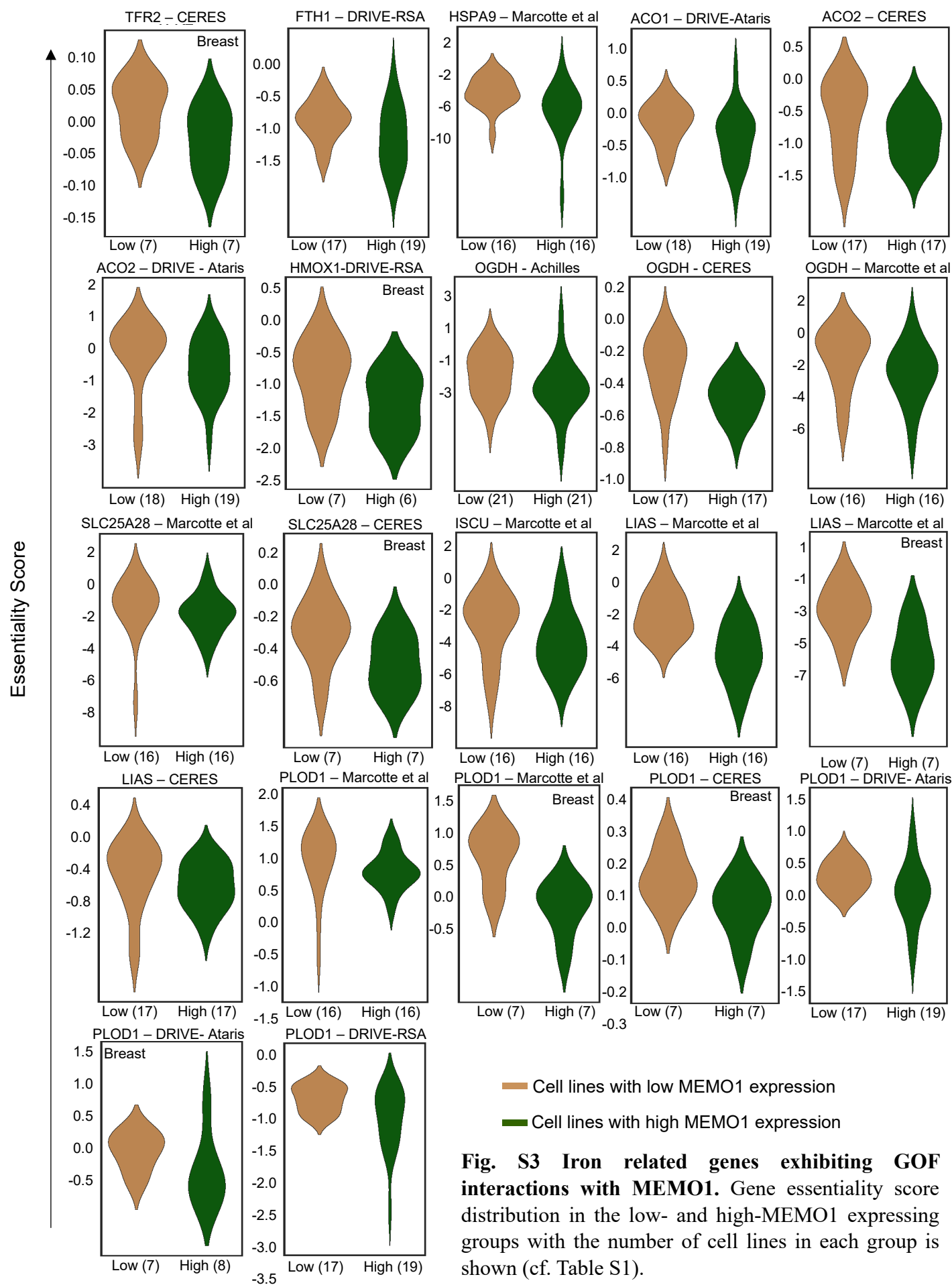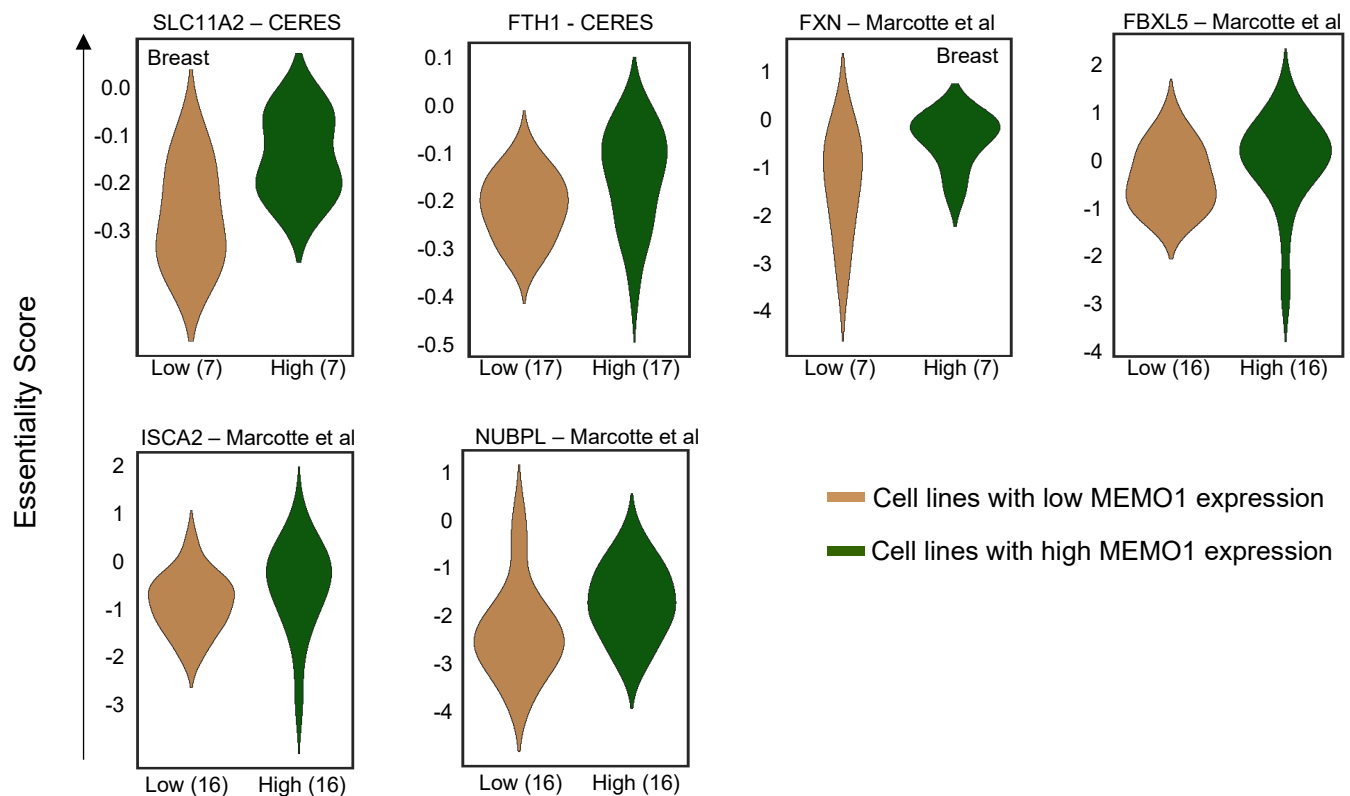
Fig. S4 Iron related genes exhibiting LOF interactions with MEMO1. Gene essentiality score distribution in the low- and high-MEMO1 expressing groups with the number of cell lines in each group is shown (cf. Table S2).
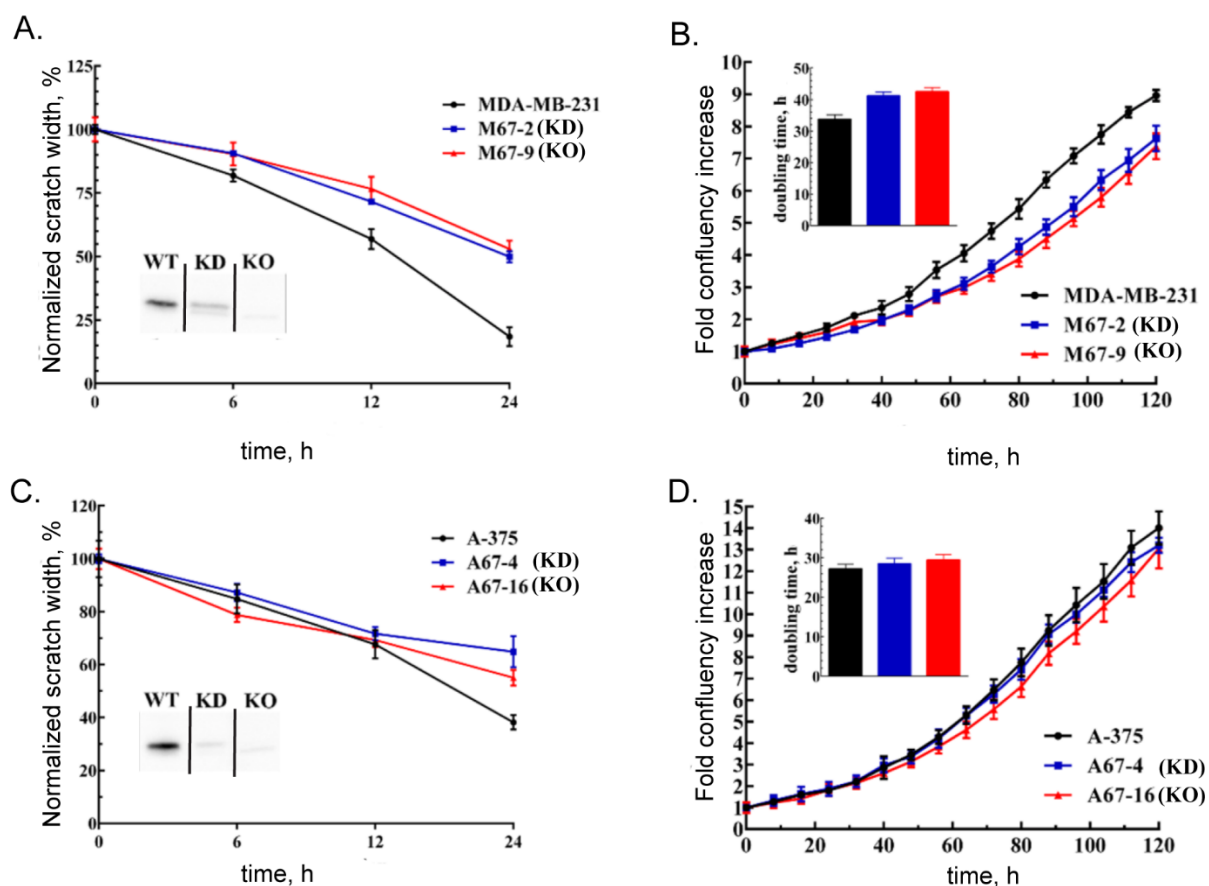
Fig. S5. MEMO1 knockout and knockdown in breast cancer and melanoma cell lines result in decrease in cellular motility and cell growth rate. (A) Wound healing assay for breast cancer cell lines MDA-MB-231 (parental), M67-2 (MEMO1 knockdown) and M67-9 (MEMO1 knockout). MEMO1 Western blots demonstrating MEMO1 expression levels in the parental cell line (WT) and in the CRISPR/Cas9 knockdown (KD) and knockout (KO) are shown in the inset. (B) Growth curves of MDA-MB-231, M67-2 and M67-9 cells. (C) Wound healing assay for A-375, A67-4 (MEMO1 knockdown) and A67-16 (MEMO1-knockout) cells. MEMO1 Western blots demonstrating MEMO1 expression levels in the parental cell line (WT) and in the CRISPR/Cas9 knockdown (KD) and knockout (KO) are shown in the inset. (D) Growth curves of A-375, A67-4 and A-67-16 cells.
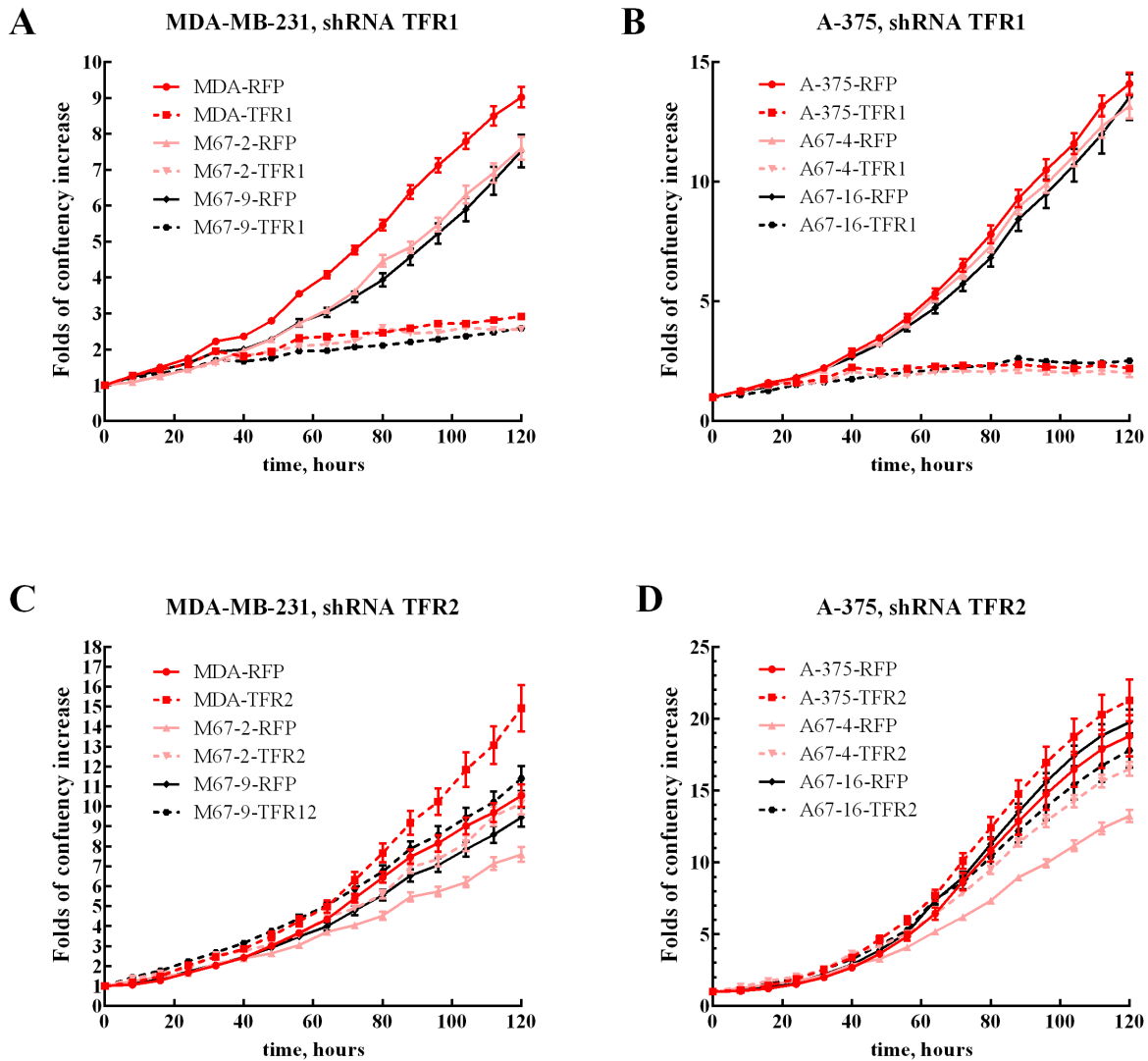
Figure S6. Growth curves of MDA-MB-231 (A, C) and A-375 (B, D) with high expression of MEMO1 (MDA-RFP and A-375-RFP, red solid lines), low expression of MEMO1 (M67-2-RFP and A67-4-RFP, pink solid lines) and no MEMO1 expression (M67-9-RFP and A67-16-RFP black solid lines), in comparison with the same cell lines transduced with TFR1 (A, B) or TFR2 (C, D) shRNA (corresponding dashed lines).
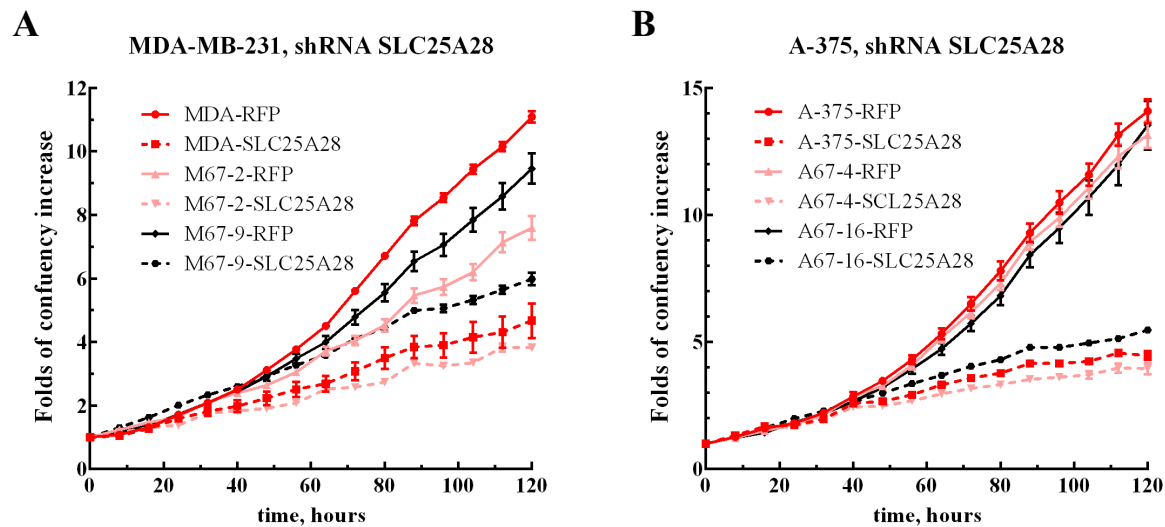
Figure S7. Growth curves of MDA-MB-231 (A) and A-375 (B) with high expression of MEMO1 (MDA-RFP and A-375-RFP, red solid lines), low expression of MEMO1 (M67-2-RFP and A67-4-RFP, pink solid lines) and no MEMO1 expression (M67-9-RFP and A67-16-RFP black solid lines), in comparison with these cell lines transduced with SLC25A28 shRNA (corresponding dashed lines).
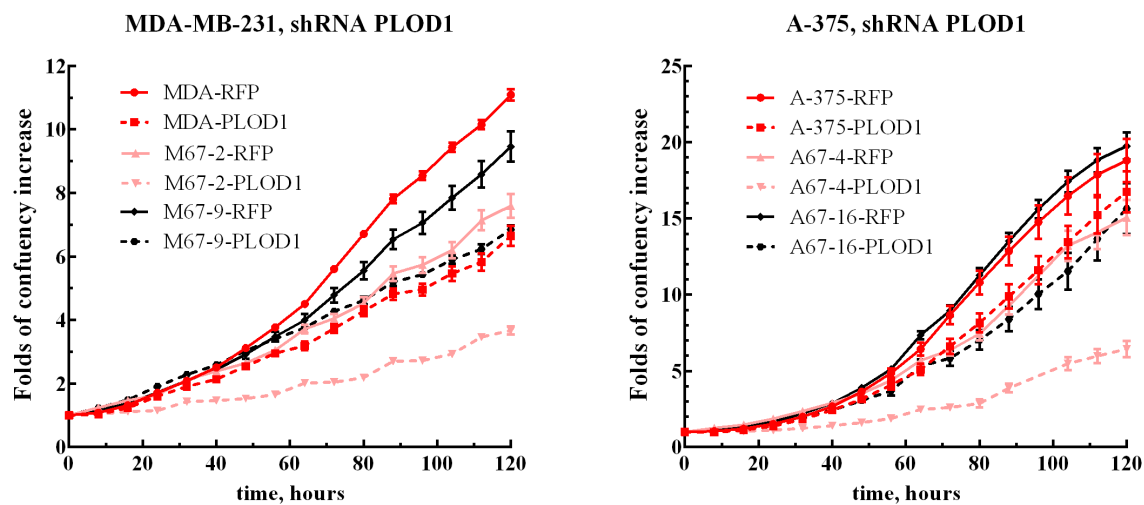
Figure S8. Growth curves of MDA-MB-231 and A-375 with high expression of MEMO1 (MDA-RFP and A-375-RFP, red solid lines), low expression of MEMO1 (M67-2-RFP and A67-4-RFP, pink solid lines) and no MEMO1 expression (M67-9-RFP and A67-16-RFP black solid lines), in comparison with these cell lines transduced with PLOD1 shRNA (corresponding dashed lines).
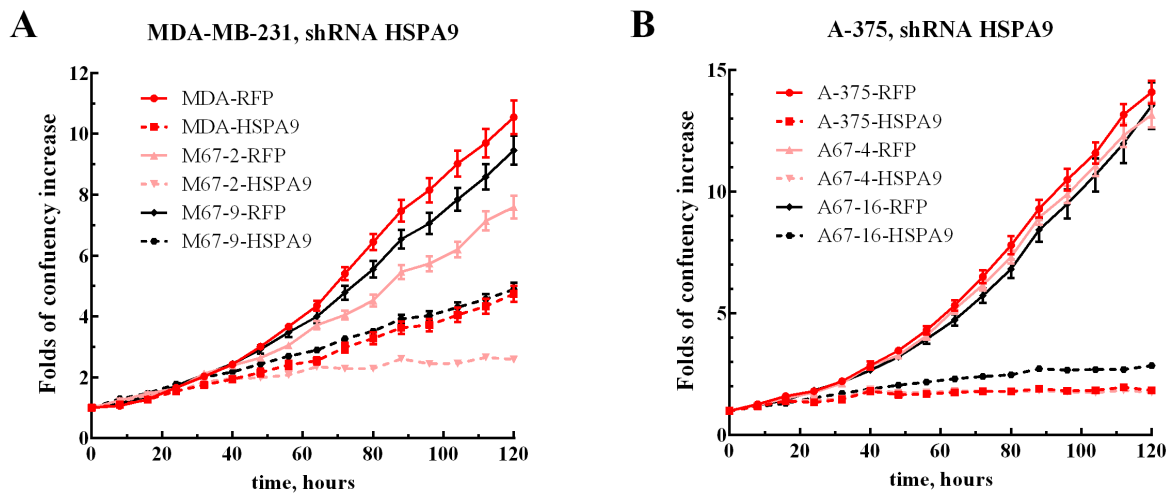
Figure S9. Growth curves of MDA-MB-231 (A) and A-375 (B) with high expression of MEMO1 (MDA-RFP and A-375-RFP, red solid lines), low expression of MEMO1 (M67-2-RFP and A67-4-RFP, pink solid lines) and no MEMO1 expression (M67-9-RFP and A67-16-RFP black solid lines), in comparison with these cell lines transduced with HSPA9 shRNA (corresponding dashed lines).
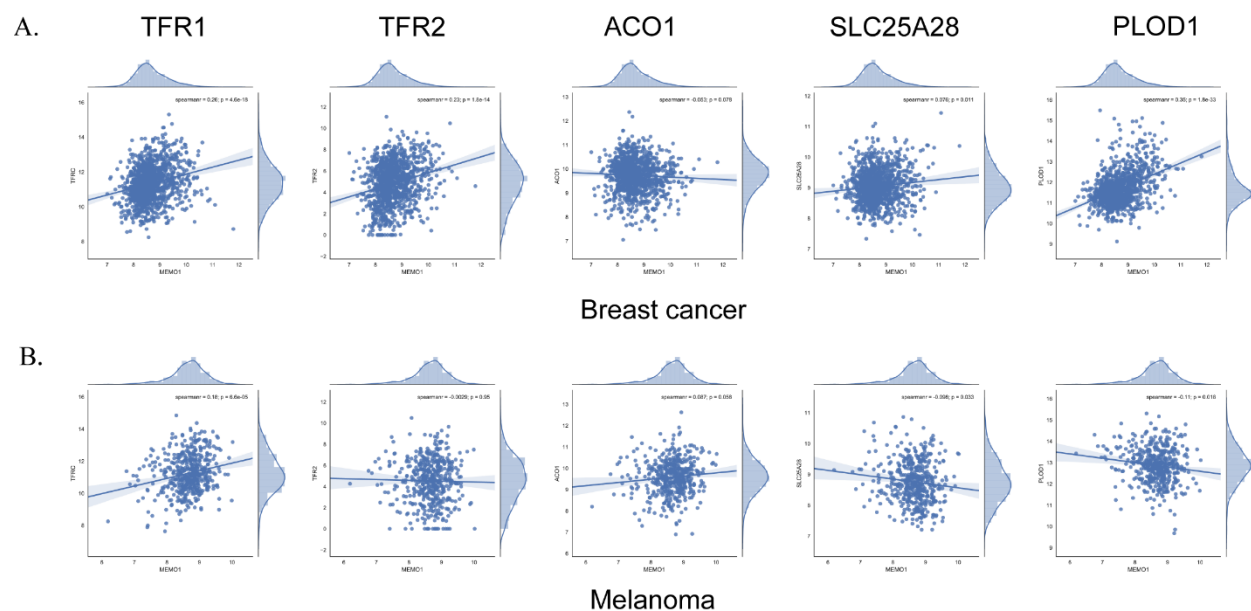
Figure S10. Correlation between the expression levels of MEMO1 and other iron related proteins in breast cancer (A) and melanoma (B) cell lines.
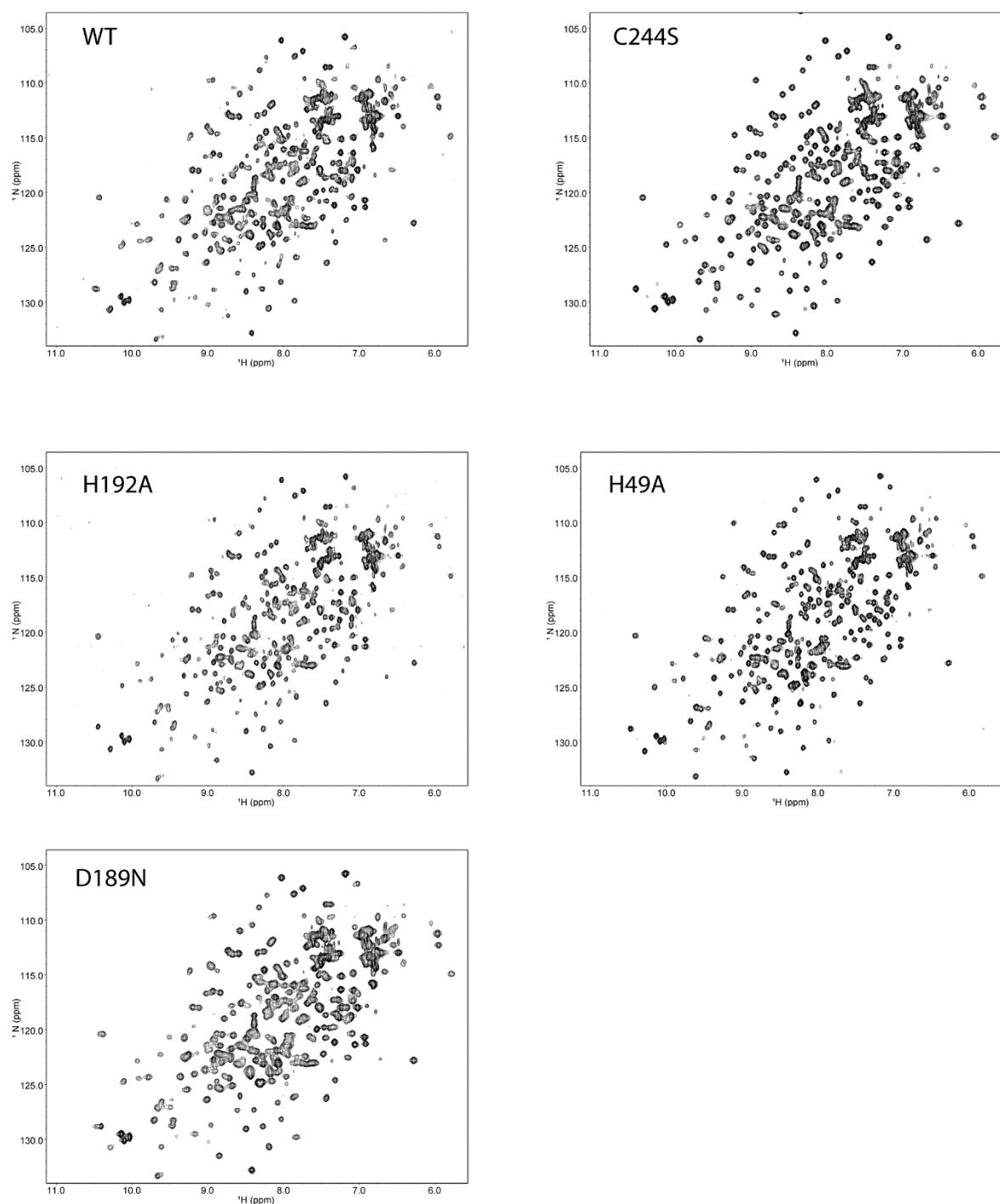
Fig. S11. Fingerprint ^{1}H,^{15}N-TROSY spectra of the wild type MEMO1 and several metal binding site mutants recorded at 900 MHz Pproteins were isotopically labeled with ^{15}N by substituting ^{15}NH$_4$Cl for the natural abundance NH$_4$Cl in the M9 medium used for protein expression. NMR samples contained 0.1 mM protein in 50 mM HEPES-Na, pH 7.4, 150 mM NaCl, 5 mM TCEP, 5% v/v D$_2$O, and 0.25 mM 2,2-dimethyl-2-silapentane-5-sulfonate. The 2D ^{1}H,^{15}N-TROSY spectra were collected on a 900 MHz Bruker Avance III spectrometer equipped with a cryogenic triple-resonance probe at a sample temperature of 298 K.
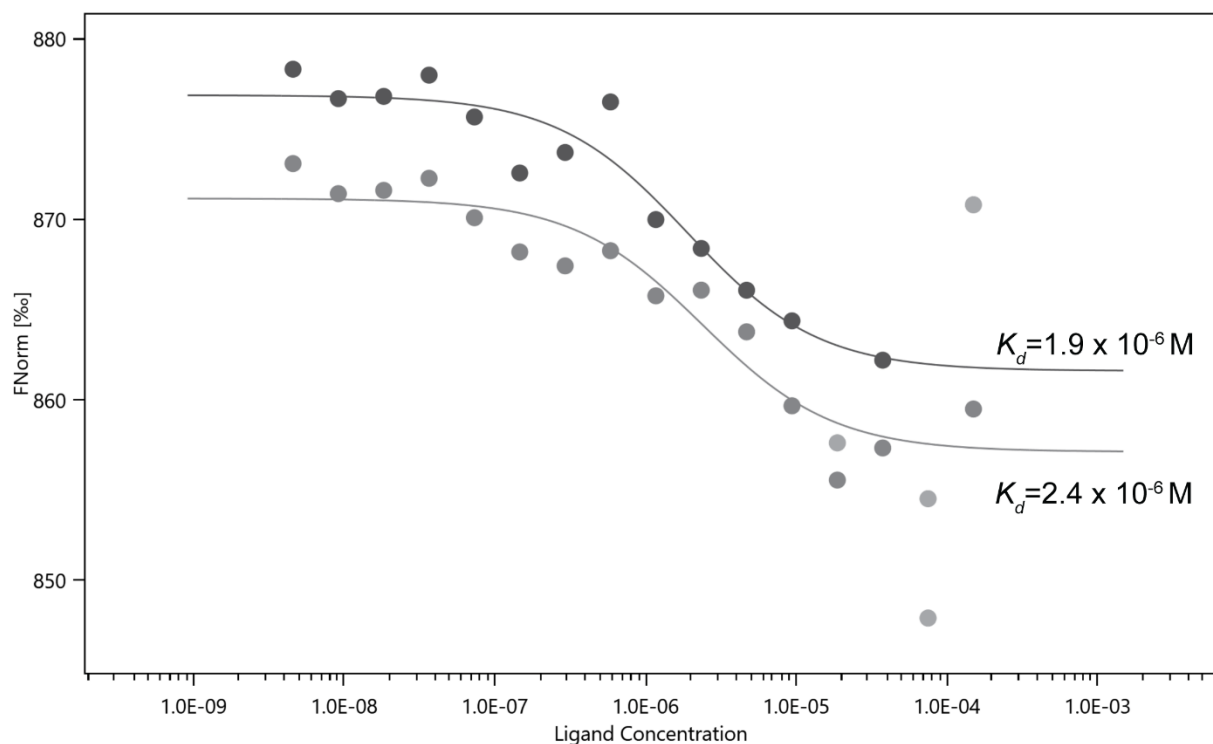
Fig. S12 Iron binding to the wild type MEMO1 analyzed by microscale thermophoresis. Two independent experiments with calculated K_d values are shown.
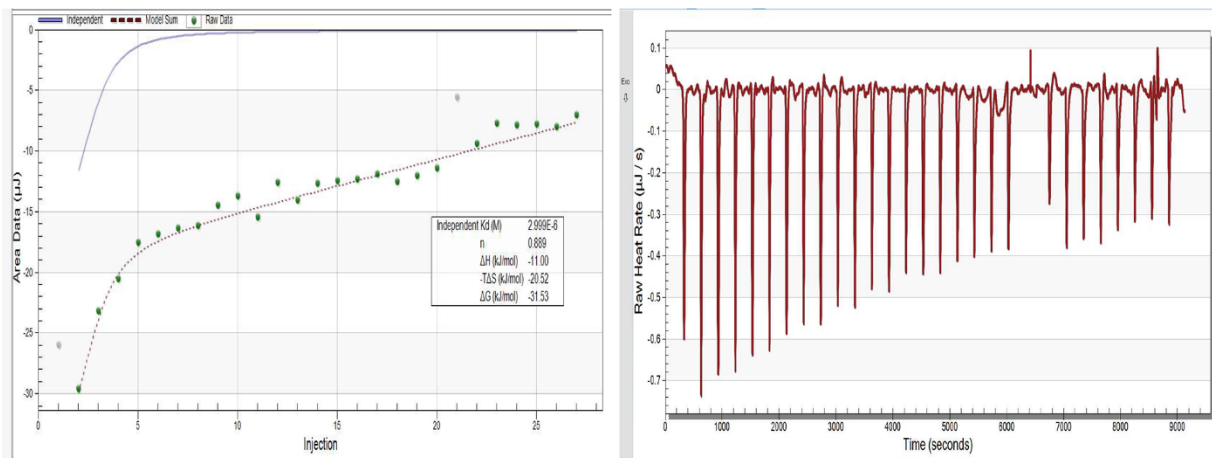
Fig. S13 Copper binding to the wild type MEMO1 analyzed by isothermal titration calorimetry.

Supplementary table S1. Iron-related genes exhibiting GOF interactions with *MEMO1*.

Gene	GO Slim	P-value	Distance low-high	Protein name	Database	Protein function
TFR2	Ion regulation	0.032	0.06	Transferrin receptor 2	CERES breast	Iron transport
FTH1	Immune System process	0.037	0.19	Ferritin H1	DRIVE -RSA, pan-cancer	Cellular iron storage
HSPA9	Chaperone and Protein folding	0.007	0.77	Mitochondrial HSP70, Grp75, mortalin	Marcotte et al, pan-cancer	Iron-sulfur cluster biogenesis
ACO1	Metabolism	0.019	0.16	Apo-form: Iron-response protein (IRP); holo-form: Aconitase	DRIVE -Ataris, pan-cancer	Iron binding protein, aconitase/IRP
ACO2	Metabolism	0.038	0.32	Mitochondrial aconitase	CERES, pan-cancer	Fe_4S_4-cluster protein, TCA cycle
		0.032	0.66		DRIVE -Ataris, pan-cancer	
HMOX1	DDR pathway & NA metabolism	0.043	0.51	Heme oxygenase 1	DRIVE -RSA, Breast	First enzyme of heme catabolism
OGDH	Mitochondrial organization	0.036	0.62	2-oxoglutarate dehydrogenase	Achilles, pan-cancer	TCA cycle, regulates HIF1α
		0.002	0.22		CERES, pan-cancer	
		0.038	1.07		Marcotte et al, pan-cancer	
SLC25A28	Mitochondrial organization	0.041	0.59	Mitoferrin-2	Marcotte et al, pan-cancer	Mitochondrial iron transport
		0.042	0.21		CERES, Breast	
ISCU	Mitochondrial organization	0.023	1.78	Iron-sulfur cluster assembly enzyme	Marcotte et al, pan-cancer	[Fe-S] cluster synthesis
LIAS	Mitochondrial organization	0.0003	1.63	Lipoic acid synthase	Marcotte et al, pan-cancer	Fe_4S_4-cluster containing protein, lipoate synthesis, regulates HIF1α
		0.009	1.74		Marcotte et al, breast	
		0.041	0.18		CERES, pan-cancer	
PLOD1	Protein modification	0.045	0.41	Procollagen-lysine,2-oxoglutarate 5-dioxygenase 1	Marcotte, pan-cancer	Iron binding protein, regulates collagen synthesis, cross-linking, and deposition
		0.006	0.53		Marcotte, breast	
		0.042	0.07		CERES, breast	
		0.013	0.24		Ataris, pan-cancer	
		0.043	0.41		DRIVE -Ataris, Breast	
		0.010	0.21		DRIVE -RSA, pan-cancer	

Supplementary table S2. Iron related genes exhibiting LOF interactions with *MEMO1*.

Genes	GO Slim	P-value	Distance low-high	Protein name	Database	Protein function
SLC11A2	Apoptosis	0.024	-0.07	DMT1	CERES, breast	Iron transport
FTH1	Immune System process	0.017	-0.09	Ferritin H1	CERES pan-cancer	Iron storage
FXN	Mitochondrial organization	0.032	-0.79	Frataxin	Marcotte et al, breast	[Fe-S] cluster biogenesis in mitochondria
FBXL5	Miscellaneous	0.038	-0.57	F-box/LRR-repeat protein 5	Marcotte et al, pan-cancer	regulates iron homeostasis
ISCA2	Mitochondrial organization	0.038	-0.39	[Fe-S] cluster assembly 2 homolog	Marcotte et al, pan-cancer	[Fe-S] cluster biogenesis in mitochondria
NUBPL	DDR pathways & NA metabolism	0.013	-0.69	Iron-sulfur protein NUBPL	Marcotte et al, pan-cancer	[Fe-S] cluster biogenesis in mitochondria

Supplementary table S3. Genes involved in ferroptosis and exhibiting GOF or LOF interactions (highlighted in light blue) with *MEMO1*.

Genes	GO Slim	P-value	Distance low-high	Protein name	Database	Protein function
TFR2	Ion regulation	0.032	0.06	Transferrin receptor 2	CERES, breast	Iron transport
FTH1	Immune System process	0.037	0.19	Ferritin H1	DRIVE - RSA, pan-cancer	Cellular iron storage
ACO1	Metabolism	0.019	0.16	Apo-form: Iron-response protein (IRP); holo-form: Aconitase	DRIVE-Ataris, pan-cancer	Iron binding protein, aconitase/IRP
VDAC1	Ion Regulation	0.0486	0.693	Voltage-dependent iron channel 1	Marcotte, pan-cancer	Transport of small hydrophilic molecules; regulation of cell volume and apoptosis
VDAC3	Ion regulation	0.032	0.452	Voltage-dependent iron channel 3	Marcotte breast	Transport of small hydrophilic molecules; regulation of cell volume and apoptosis
SLC25A28	Mitochondrial organization	0.041	0.59	Mitoferrin-2	Marcotte, pan-cancer	Mitochondrial iron transport
		0.042	0.21		CERES, breast	
ACSL4	Metabolism	0.040	0.248	Acyl-CoA Synthetase Long Chain Family Member 4)	Achilles pan-cancer	Lipid metabolism
SIRT3	unknown	0.005	0.839	Sirtuin-3	Marcotte pan-cancer	NAD-dependent deacetylase
		0.042	0.554		Marcotte breast	
		0.009	0.539		Achilles pan-cancer	
SCO2	Mitochondrial organization	0.001	0.149	Sco2	CERES pan-cancer	Mitochondrial copper chaperone
ALOXE3	metabolism	0.030	0.063	Hydroperoxide isomerase ALOXE3	CERES pan-cancer	Non-Heme iron-containing lipoxygenase
PTGS2	*Intracellular Protein Traffic*	0.042	0.038	prostaglandin-endoperoxide synthase 2	CERES breast	Prostanoid biosynthesis

FXN	Mitochondrial organization	0.032	0.787	frataxin	Marcotte breast	[Fe-S] cluster biogenesis in mitochondria
CS	Metabolism	0.048	-0.236	Citrate synthase	Ataris pan-cancer	TCA cycle
ACSL4	Metabolism	0.042	-0.418	Acyl-CoA Synthetase Long Chain Family Member 4)	Marcotte breast	Lipid metabolism
SCP2	Cell cycle and Mitosis	0.024	-0.651	sterol carrier protein 2	Marcotte breast	Intracellular lipid circulation and metabolism
GLS2	Mitochondrial organization	0.013	0.129	Glutaminase 2	CERES breast	Glutamine catabolism, mitochondrial respiration
SCO2	Mitochondrial organization	0.042	0.744	Sco2	Marcotte breast	Mitochondrial copper chaperone
		0.022	-1.32		Achilles breast	
FH	Mitochondrial organization	0.014	-0.328	Fumarate hydratase	Atares pan-cancer	TCA cycle
ALOX12	Metabolism	0.044	0.049	arachidonate lipoxygenase	CERES pan-cancer	Lipid peroxidation

Supplementary Table S4

Structure determination statistics for MEMO1-metal complexes and the C244S mutant

	MEMO1 WT – Fe^{2+}	MEMO1 WT – Cu	MEMO1 C244S - Cu
Wavelength	1.03320	0.97933	0.98011
Resolution range	47.82 – 2.15 (2.23-2.15)	42.91- 2.55 (2.64 – 2.55)	42.1 – 1.75 (1.81 – 1.75)
Space group	$P\,2_12_12$	$P\,2_12_12$	$P\,2_12_12$
Unit cell (Å)	a = 139.64 b = 88.86 c = 97.36	a = 140.63 b = 87.16 c = 98.59	a = 140.00 b = 89.52 c = 97.54
Reflection measured	880,581 (85,505)	597,689 (76,841)	1,834,535 (291,514)
Unique reflections	66,565 (6570)	40,211 (3967)	123,799 (20,426)
Multiplicity	13.2 (13.0)	14.86 (19.37)	14.82 (14.27)
Completeness (%)	99.9 (99.91)	99.82 (99.87)	99.86 (99.68)
Mean I/sigma (I)	19.14 (5.88)	16.56 (3.13)	27.83 (3.2)
Wilson B-factor	22.78	35.23	18.82
R-merge	0.1351 (0.5015)	0.186 (1.09)	0.088 (1.05)
CC 1/2	0.998 (0.968)	0.998 (0.886)	1.0 (0.893)
Reflections used for refinement	66,518 (6564)	40,172 (3962)	123,704 (12, 178)
R-work	0.16 (0.20)	0.19 (0.28)	0.16 (0.26)
R-free	0.20 (0.25)	0.25 (0.32)	0.19 (0.30)
Non-hydrogen atoms	10,319	9286	11239
Protein residues	1178	1171	1176
RMS (bonds)	0.006	0.003	0.009
RMS (angles)	0.83	0.51	0.94
Ramachandran plot Favored (%)	98.12	97.51	98.37
Allowed (%)	1.88	2.49	1.63
Outliers (%)	0	0	0
Rotamer outliers (%)	1.2	3.94	1.99
Clashscore	3.46	3.33	2.46
Average B-factor	26.46	44.79	22.70
No of TLS groups	4	4	4
PDB code	7KQ8	7L5C	7M8H

Materials and Methods supplementary information.

Antibody and Western blotting details: The following antibodies were used: anti-Memo1 antibodies (mouse monoclonal antibodies AT1E9, sc-517412, Santa Cruz Biotechnology, dilution 1:500 in 0.5% of blocking reagent on PBST), anti-PLOD1 (LLH1) antibodies (mouse monoclonal antibodies B-5, sc-271640, Santa Cruz Biotechnology, dilution 1:500 in 0.5% of blocking reagent on PBST), anti-OGDH antibodies (rabbit polyclonal antibodies PA5-28195, Invitrogen, dilution 1:2,000 in 0.5% of blocking reagent on PBST), anti-TfR1 antibodies (mouse monoclonal anti-CD71 antibodies 3B8 2A1, Santa Cruz Biotechnology, dilution 1:500 in 0.5% of blocking reagent on PBST), anti-TfR2 antibodies (mouse monoclonal antibodies B-6, sc-376278, Santa Cruz Biotechnology, dilution 1:100 in 0.5% of blocking reagent on PBST), anti-Aco1 antibodies (rabbit polyclonal antibodies PA5-41753, Invitrogen, dilution 1:1,000 in 0.5% of blocking reagent on PBST), anti-SCL25A28 (rabbit polyclonal antibodies against mitoferrin 2, BS-7157R, Bioss, ThermoFisher Scientific, dilution 1:500 in 0.5% of blocking reagent on PBST), anti-Grp75 antibodies (mouse monoclonal anti-HSPA9 antibodies D-9, sc-133137, Santa Cruz Biotechnology, dilution 1:1,000 in 0.5% of blocking reagent on PBST), anti-actin β antibodies (MA5-15452, Invitrogen, dilution 1:10,000 in 0.5% of blocking reagent on PBST). Following incubation with primary antibodies, membranes were washed in 0.5% blocking reagent on PBST three times for 5 minutes, and incubated with the following secondary antibodies for 1 hour at room temperature: Amersham™ ECL™ Anti-Mouse IgG, Horseradish Peroxidase (HRP)-Linked Species-Specific Whole Antibody (from sheep) (NA931V), dilution 1:1,000, or Pierce donkey anti-rabbit HRP-linked antibodies (#PI31458), dilution 1:2,500. Membranes probed with anti-TfR2 antibodies were incubated with m-IgGk BP-HRP secondary antibodies (Santa Cruz, sc-525409, dilution 1:1,000).

Site-directed mutagenesis details: To generate MEMO1 binding site variants, QuickChange method (Agilent) was used with the following primers:

Mutation	Primer sequence
H49A	GCG ATT ATC GCG CCA GCG GCG GGC TAT ACT TAC TG CAG TAA GTA TAG CCC GCC GCT GGC GCG ATA ATC GC
H192A	CAT CCG ATT TCT GCG CGT GGG GCC AGC GTT TC GAA ACG CTG GCC CCA CGC GCA GAA ATC GGA TG
D189N	CAT CCG ATT TCT GCG CGT GGG GCC AGC GTT TC GAA ACG CTG GCC CCA CGC GCA GAA ATC GGA TG
C244S	CTT AAA AAA TAC CAC AAT ACG ATC TCT GGT CGC CAT CCA ATC G CGA TTG GAT GGC GAC CAG AGA TCG TAT TGT GGT ATT TTT TAA G

CRISPR knockout details: To generate MEMO1 knockouts, CRISPR1006367_SGM sgRNA (Thermo Fisher Scientific) was used with the target DNA sequence TACGGAGAACTGTGGAAGAC, and the protospacer adjacent motif AGG. Primers

ACATACCCACATACACTCAC and CCTCCTTCCTTTCCTTTCTTTC were used to amplify the region of genomic DNA targeted for cleavage by this sgRNA, and the subsequent genomic cleavage detection.